Přírodovědecká fakulta
Univerzita Palackého v Olomouci

Katedra experimentální fyziky

Bakalářská práce

Relativní kalibrace fluorescenčního teleskopu projektu FAST

Autor	Koutný Michal
Vedoucí práce	Mgr. Dušan Mandát Ph.D.
Studijní obor	Nanotechnologie
Forma studia	Prezenční
Rok	2021

Bibliografická identifikace

Jméno a příjmení autora	Koutný Michal
Název práce	Relativní kalibrace fluorescenčního teleskopu projektu FAST
Typ práce	bakalářská
Pracoviště	Katedra experimentální fyziky
Vedoucí práce	Mgr. Dušan Mandát Ph.D.
Rok obhajoby práce	2021
Počet stran	49
Počet příloh	1
Jazyk	anglický
Abstrakt	The Fluorescence detector Array of Single-pixel Telescopes (FAST) je koncept moderní observatoře určenou pro detekci vysoko-energetickcýh kosmických částic. Tato práce pokládá teoretický základ pro ultra vysoko-energetické kosmické záření (UHECR), FAST projektu a dalekohledů, optických a elektrických komponentů přítomných na zmíněném teleskopu a popisu jeho kalibračního systému. Porovnáním signálu ze čtyř fotonásobičů (PMTs) situovaných na dalekohledu byla provedena datová analýza týkající se především relativní kalibrace fotonásobičů. Kladen důraz je na jejich časovou a teplotní stabilitu. Všechna použítá data pramení z UV LED kalibračních měření a pochází z reálných měření provedených v Observatoři Pierra Augera v Argentině.
Klíčová slova	kosmické záření, UHECR, EAS, FAST projekt, fotonásobič, relativní kalibrace

Bibliographical identification

Author's first name and surname	Koutný Michal
Title	Relative calibration of fluorescent telescopes of the FAST project
Type of thesis	bachelor
Department	Department of Experimental Physics
Supervisor	Mgr. Dušan Mandát Ph.D.
Year of presentation	2021
Number of pages	49
Number of appendices	1
Language	english
Abstract	The Fluorescence detector Array of Single-pixel Telescopes (FAST) is a concept for next generation observatory of high energy cosmic particles. This thesis lays the theoretical foundations for ultra high-energy cosmic radiation (UHECR), the FAST project and telescopes, the optical and electrical components present on said telescopes and its calibration system. By comparing the signal of four Photomultiplier Tubes (PMTs) stationed on the telescope, data analysis concerning relative calibration of the PMTs was performed. Of particular importance is their stability with respect to both time and temperature. All data utilized was obtained from UV LED calibration measurements and originate from real in-situ measurements from the Pierre Auger Observatory, Argentina.
Keywords	cosmic radiation, UHECR, EAS, FAST project, photomultiplier tube, relative calibration

Prohlášení

Prohlašuji, že jsem předloženou diplomovou práci vypracoval samostatně pod vedením Mgr. Dušana Mandáta Ph.D. a že jsem použil zdrojů, které cituji a uvádím v seznamu použitých zdrojů.

V Olomouci dne .....

.....
podpis

Chtěl bych poděkovat vedoucímu bakalářské práce Mgr. Dušanu Mandátovi, Ph.D. za čas, nesmírnou trpělivost a odhodlání při tvorbě této práce. Dále bych chtěl poděkovat Mgr. Petru Hamalovi, Ph.D. za cenné rady ohledně Python skriptů a práci s FAST databází.

Table of Contents

Introduction

The Fluorescence detector Array of Single-pixel Telescopes (FAST) is a concept for next generation observatory of high energy cosmic particles. The energy of ultra high-energy cosmic radiation (UHECR) ranges from 10^{18} to 10^{20} eV. Detection of such radiation is exceptionally problematic, as the minute flux of such high-energy rays, meaning the frequency at which they hit the surface of the Earth, is ~ 1 particle per km^2 per century. For that reason, a large net of telescopes has to be deployed in order to obtain any sufficient amount of data for proper statistical analysis.

Currently two methods of detection are utilized. Surface detectors use scintillation of secondary particles produced by a UHECR interacting with particles in Earth's atmosphere. Fluorescence detectors observe faint fluorescent UV light produced by excitation and subsequent deexcitation of nitrogen atoms in the atmosphere. The incident cosmic ray produces an extensive air shower (EAS) of secondary particles which can be detected. Both methods can be used in coincidence, such as is the case with Telescope Array (TA), Utah - USA and Pierre Auger Observatory (PAO), Argentina.

FAST project uses fluorescence-based telescopes. Taking into effect the low flux of UHECRs, a large grid of fluorescent telescopes has to be deployed for proper land coverage. Low economic cost of a FAST telescope is one the essential demands of the project. Furthermore, the telescope is required to have an aperture collecting area of 1 m^2, with a field of view (FOV) of $30° \times 30°$. For light detection, the telescope utilizes a 2×2 matrix of four 200mm Photomultiplier Tubes (PMTs). After a successful proof of concept run, several FAST telescopes were deployed on both TA and PAO sites.

Calibration is of vital importance for the operation of these telescopes. A telescope in PAO, Argentina is equipped with a UV LED flasher on its central circular mirror. By comparing the signal values from all four PMTs with one of the PMTs chosen as a reference point, a procedure called relative calibration has been performed. Temperature shift, material deterioration or parasitic background radiation for example can cause signal alteration in absolute numbers, as the variations affect all four PMTs equally. By comparing the individual PMTs on a single FAST telescope, the relative values should in theory stay stabilized. This can provide information about the behaviour of each PMT in relation to each other.

The aim of this thesis is the analysis of the UV LED calibration measurements from the Pierre Auger Observatory in Argentina, with particular importance on relative calibration. The fundamental goal is to assess the environmental impact to the FAST instrumentation and its influence on the relative calibration done by comparison of the signal from all four PMTs, primarily with respect to both time and temperature. The thesis discusses the current status and future improvements of the methods within the FAST telescope.

1. Foundations

1.1. Cosmic radiation

Cosmic radiation is the natural space radiation hitting the Earth every single second. These rays consist primarily of high-energy protons and atomic nuclei travelling through space at nearly the speed of light. The closest and for us the most important source of these particles is the Sun. These rays can also originate in our own galaxy, supernova explosions or in mysterious processes in distant galaxies. Ordinarily, these mostly positively charged energetic particles are deflected by the Earth's strong magnetic field. But that is not always the case. For example, because the magnetic field produced by the core of our planet is weakest at the poles, ionization of atmospheric particles precisely by the cosmic radiation can occasionally produce beautiful and breathtaking auroras. But if the particle itself has enough velocity, and subsequently enough energy, it can power through the Earth's magnetic shield and cause faint fluorescent light shows everywhere on Earth.

Cosmic radiation can be quantified and differentiated by the origin of the particle, charge, but also the energy of the incident cosmic ray charging towards the Earth. Various units of energy are utilized to assess such radiation, the most widespread and also the one most fitting for the purpose of describing high-energy particles are electronvolts (eV). An electronvolt is the amount of kinetic energy an electron gains if placed in an electric potential difference of one Volt in a vacuum. However, an electronvolt is a unit too small to properly assess cosmic rays. For that reason characterization of the energy of cosmic radiation will be done in powers of eV. Another important aspect to be used in evaluation of these particles is their minute flux. That is, the frequency at which they shower the surface of the Earth.

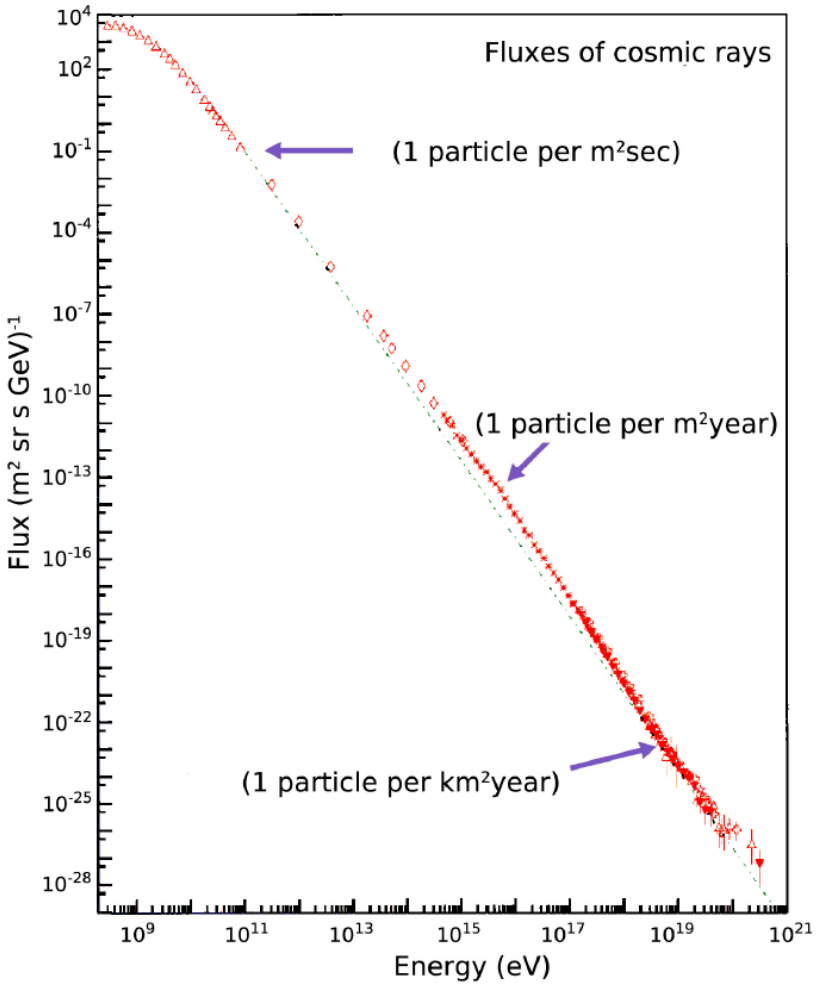

Figure 1 | Relation between the energy and the flux of cosmic radiation. [1]

The flux of incoming cosmic rays is not constant. It varies depending on several terrestrial and even extraterrestrial attributes. As mentioned beforehand, the Earth's magnetic field is a significant factor in particle physics. The stronger the field, the harder it is for the particle to charge through this planetary defense shield. Furthermore, elevation has to be taken into consideration when detecting these rays. The higher the altitude, the less atmospheric mass there is between us and the particle itself, which means the probability of absorption decreases and subsequently, the probability of detection increases. As for the extraterrestrial aspect, it is indicated that minute flux of cosmic radiation is correlated with solar activity. Solar wind may play a crucial role as a barrier to the radiation. The frequency of cosmic rays is rapidly reduced following the increase of its energy, as shown in figure 1. Looking at the most energetic radiation there is, 10^{18} to 10^{20} eV, there is no theoretical background as to what in the universe can generate particles of such massive energies. And because of its extremely low minute flux, a particle per square kilometer per century, understanding the processes that lead to formation of these cosmic rays proved troublesome. [1]

1.1.1. UHECRs

While discoveries throughout the last 50 years have given us great insight to both nature and origin of regular cosmic rays, understanding of their more energetic variations is still limited. These ultrahigh-energy cosmic rays (UHECRs) are to this day an elaborate mystery to the scientific community. The energy of such particles is measured in powers of electronvolts. For a cosmic particle to be considered a UHECR, it has to come charging at the Earth with energies anywhere between 10^{18} to 10^{20} eV. The most powerful particle accelerator on Earth, Cern's Large Hadron Collider, is only capable of conceiving particles with energies up to 10^{13} eV. Which means that somewhere in the universe, probably not even within our own galaxy, something is creating particles that are million times more energetic than anything we can produce on Earth. To understand this phenomenon would be to forever change high energy physics and how we think of extragalactic space.

Regular cosmic rays are composed primarily of protons stripped from their atomic shelves with some alpha particles and a minority of different particles [2]. Because these particles are charged, either positively, as in protons and atomic nuclei, or negatively, as in electrons, during their travels they are inevitably deflected due to various magnetic fields they encounter. Which means their paths are altered and their origin is no longer traceable. These kinds of particles appear to hit the Earth from every direction in the sky. That is no longer the case with UHECRs. During their creation, they are accelerated to incredible magnitudes, to almost the speed of light. Because of their massive energies, they are able to power through most magnetic fields and only get deflected by a few degrees at most [3]. Therefore, tracking these particles to their point of origin is feasible, to improve our understanding of the events that led to formation of such energetic particles.

Upon UHECR entering the Earth's atmosphere, a cascade of secondary particles is generated. When an energetic particle hits an atom, it produces many hadrons with less energy that the primary particle, but still energetic enough for this process to repeat various times. Such a cascade of particles is called an extensive air shower (EAS). The EAS results in mainly Cherenkov and fluorescent photons from the deexcitaion of nitrogen atoms in the Earth's atmosphere. These photons fall into the UV portion of the spectrum (300 nm – 420 nm) and can be detected using ground-based telescopes. The largest concern of such telescopes is the scarcity of UHECRs. On average, only one such particle hits the Earth per square kilometer per century.

1.2. Detection of UHECRs

Because of the exceptionally low flux, a telescope area covering a huge amount of land has to be constructed in order to obtain any meaningful sample for proper statistical analysis. Therefore, it is no longer plausible to use satellites or balloons to detect these high-energy cosmic particles in a way that is utilized with their lower energy counterparts. At this moment, two facilities fulfil the set criteria. The Telescope Array experiment in Utah - USA, spanning 700 km^2 and the Pierre Auger Observatory spanning 3000 km^2 in Argentina. Both projects offer appropriate coverage of land with a surface grid containing a large number of telescopes.

Both these sites use a combination of two detection techniques to maximize the rate of observation of these scarce cosmic rays. One of the used methods is fluorescence detection, where UV fluorescent photons are detected by a large ground-based telescope. The other method being surface detection, where the density of secondary particles created through an EAS is measured as the particles themselves hit the Earth's surface.

1.2.1. Fluorescence detectors

When a UHECR comes charging at the Earth and enters its atmosphere, it interacts with the individual atoms that the atmosphere is composed of. This usually means nitrogen atoms, as they account for ~ 78 % of the air surrounding us. Upon the interaction itself, the collision excites the nitrogen atom, which after a brief period of time emits an Ultra-Violet (UV) photon. Following the emission, the UV photon travels to the surface of the Earth, where hopefully it hits one of the many ground-based telescopes in a given observatory. The telescopes use large, curved, highly reflective mirrors, which causes the UV radiation to be reflected and focused onto individual pixels comprised of Photomultiplier Tubes (PMTs), where the faint signal is amplified and subsequently analysed.

Photomultiplier Tubes are very sensitive, as they can easily magnify a given signal thousandfold. Therefore, light shielding is vital for proper operation, as any parasitic electromagnetic radiation will easily damage the gadgets. This means the telescope has to operate in near absolute darkness. Any man-made light has to be limited. Furthermore, because of the high sensitivity of PMTs, the telescope can operate only during clear and moonless nights, as the large amount of light from the moon itself will severely hinder the detection capabilities of the detector. Humidity is an important factor when discussing the efficiency of fluorescent telescopes as well. Dry air is required for proper function as aerosols present in the atmosphere cause light dispersion and absorption, limiting the performance factor of the telescopes.

Although fluorescence detection is a powerful technique, a single telescope can only offer information on the intensity of the UV radiation. To obtain any information about the original direction of UHECRs, signal from multiple detectors is essential. For that reason stereoscopic mode is used. Much like our eyes, which also utilize this specific mode, the telescope itself sees only a plane upon the UV photon hitting the mirror. By combining information gathered from at least two individual telescopes at two distinct locations, a 3D image of the original cosmic ray can be constructed. If two telescopes see the same EAS, intersection of the observed planes provides the necessary data. From that, estimation of the primary direction of UHECRs can be developed.

1.2.2. Surface detectors

When a UHECR produces an air shower, countless other particles are formed. These secondary particles eventually reach the ground, where they get detected with the usage of hundreds surface detectors, called scintillator detectors. They detect the density of secondary particles as they pass through the device. The timing of the detection is crucial. By looking at very small time differences (millionths of a second), an estimation may be formed regarding the arrival direction of the incident primary cosmic ray. These detectors are placed in a net throughout the whole site, to maximize the probability of detection. They function nonstop throughout the whole year.

The surface detectors in Telescope Array in Utah are composed of a detection device inside two metal sheets. The material of the device inside the sheet is designed to interact with charged particles. When a cascade of secondary particles hits the surface detector, the scintillating molecules inside the device are excited and thus emit ultraviolet light. With the usage of optical fibers, the UV light is steered onto a Photomultiplier Tube, which converts the light into an electrical signal. The information is then collected and gathered. The whole device is powered by a solar panel on top of the metal sheets. [4]

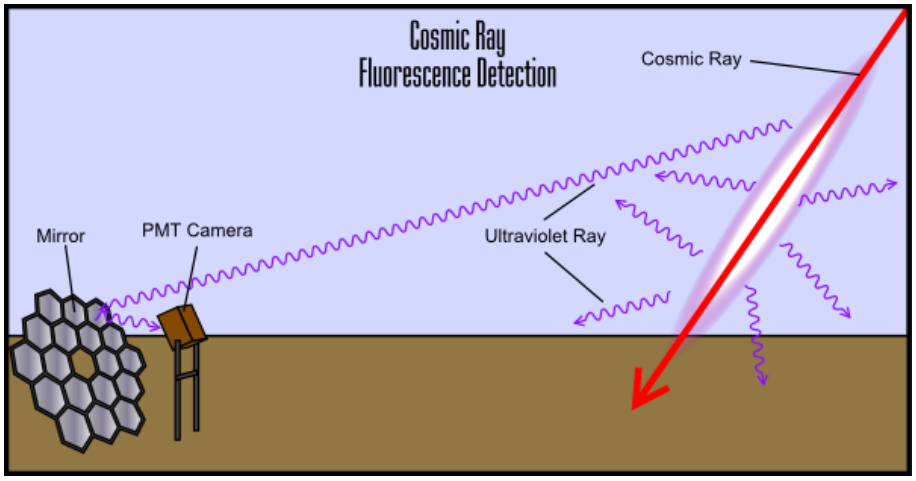

Figure 2 | An illustration of an EAS producing UV photons. [4]

The Pierre Auger Observatory employs a similar, yet distinct method. Instead of metal sheets, a barrel of highly purified water is utilized. There are about 1660 tanks in the whole 3000 km^2 of the site. Each tank can receive up to 12 000 liters. Since the speed of secondary cosmic particles is higher than the speed of light in water, upon entry of said particles Cherenkov light is produced. Due to present Photomultiplier Tubes the light can be observed and measured. A single EAS can generate billions of secondary particles, which get observed on these Cherenkov detectors. The energy of primary UHECR can be roughly determined with data gathered from a single observation from several tanks. As was the case with surface detectors in TA, time differences in measurements can be used to identify original direction of aforementioned UHECR. [5]

Figure 3 | A surface Cherenkov detector in PAO. [5]

1.2.3. TA and PAO observatories

Both Telescope Array in Utah and Pierre Auger Observatory offer large amount of land with hundreds of fluorescence and surface detectors. To compensate the exceptionally low flux of UHECRs, a large grid of both types of detectors is required to properly assess and study these energetic cosmic rays. The focus of this thesis is on The Fluorescence detector Array of Single-pixel Telescopes project, a concept for a grid of fluorescent detectors that observe UV light emitted from the deexcitation of nitrogen atoms in the atmosphere. Only detectors in PAO, Argentina will be studied.

1.3. FAST Project

The Fluorescence detector Array of Single-pixel Telescopes (FAST) is a concept for a next-generation of ground-based UHECRs observatories. Taking into effect the concerns for a large grid area of land and its low economic cost makes these types of detectors perfect for measurements of various properties of high energy cosmic rays. A single FAST telescope consists of four pixels covering a $30° \times 30°$ chunk of the sky, with a collecting aperture area of ~ 1 m^2. Each pixel is equipped with a Photomultiplier Tube to amplify the signal gained from the faint UV light produced during an EAS. The low cost of such a design would ensure the efficiency in building a large net covering a huge amount land, making it a prominent contender in the effort for next-generation UHECRs observatories.

A design such as this comes with the expense of low geometrical resolution, as single-pixel nature of the telescope does not allow for the estimated reconstruction of the incident cosmic ray. The granularity of the 2×2 matrix does not provide sufficient timing information to properly model the origin and direction of UHECRs. However, provided an adequately large net of said telescopes, a cosmic ray energetic enough would cause an air shower to be detected at multiple FAST detectors along with their surface counterparts. Timing data along with signal shape from several surface and fluorescence detectors could then prove sufficient in reconstructing the geometry of extensive air showers. [6]

While surface detectors provide accurate information regarding the distribution of secondary particles at ground level, largely due to their excellent duty cycle, they lack the accuracy in reading of UHECR energy. This is why a combination of both methods proves beneficial, as fluorescent techniques collect UV light emitted during the EAS development. This facilities a calorimetric measurement of the shower's energy. Furthermore, observation of the cascade provides information regarding the depth of maximum development ($X_{\max}$), a parameter indicative of the primary particle's mass. One major downside of fluorescent detection is its significantly lower duty cycle, along with sub-optimal directional coverage. Utilizing both EAS detection in surface and fluorescent telescopes, calorimetric readings of the shower's energy can be used to calibrate the energy scale of surface detectors. This method is known as hybrid detection and is applied in both the Telescope Array and Pierre Auger Observatory. With this technique, both TA and PAO have measured energy spectrum up to 100 EeV. [7]

A test of proof of concept of the FAST Project took place in 2014 at the Black Rock Mesa (BRM) site in TA, Utah - USA. A detector with a single 200mm PMT at the focus of two 1 m^2 fresnel lenses with a UV protective acrylic plate was used in a demonstration of feasibility of the concept. The telescope was first used in detecting ultraviolet laser rays from distances up to 21 km. Furthermore, the prototype observed 16 UHECR candidates and proved viability of such design.

In consideration with positive results from the experiment, a full sized FAST telescope has been developed. The model operates with a large segmented primary mirror with a diameter of ~ 1.6 m which focuses fluorescent UV light onto a 2×2 grid of four 200mm PMTs. Three such prototypes were deployed in Telescope Array for testing in observation of distant ultraviolet laser shots and detection of UHECRs.

1.4. FAST telescope design

With respect to the extraordinarily low flux of high energy cosmic radiation a large net of detectors has to be deployed for proper land coverage. In contemplation of requirement of hundreds of aforementioned telescopes, price affordability needs to be taken into account in development. The low-cost aspect is critical in stationing the detectors onto a large grid. For that reason, limiting the amount of optical elements is vital. In addition, maintenance, transportation and installation have to be simple and straightforward to the minimize the cost. The primary objective was to devise a telescope with $30° \times 30°$ field of view (FOV) and ~ 1 m^2 collecting area with a grid of four 200mm PMTs at which the light is focused on. Refractive, reflective and a combination of both designs were considered in development of the FAST telescope.

1.4.1. Refractive design

A refractive design of a fluorescent UHECR detector could employ a series of Fresnel lenses, such as the proof-of-concept design used in the Telescope Array experiment in 2014. Such structure would provide the simplest and cheapest telescope, but would be unable to satisfy the ~ 1 m^2 collecting area requirement, as commercially available lenses only go up to 0.6 m, offering ~ 0.36 m^2, which does not fulfil the set criteria. Furthermore, limitation of incident light angles presents a significant downside.

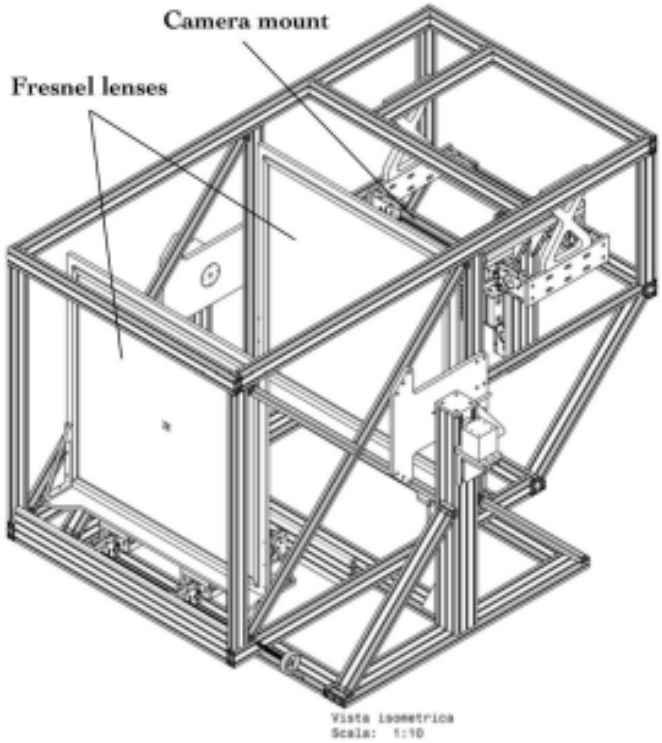

Figure 4 A fluorescent telescope employing a refractive design with two Fresnel lenses in TA, Utah. [8]

1.4.2. Reflective design

A large single or segmented mirror could easily provide the necessary sky coverage of $30° \times 30°$. A single spherical mirror of required size would inflate the overall cost of the design by a large margin. In addition, an aspherical corrector plate is mandatory to eliminate on-axis aberrations. This design is only useful for low FOV utilization. To comply with the required FOV, lacking the corrector plate a lensless Schmidt camera can be used. [9]

1.4.3. Optimal design

The optimal design of the FAST telescope utilizes a Schmidt type optical system. Ordinarily, to reduce the effect of coma, astigmatism and off-axis aberration a corrector plate is used at the entrance of the aperture of the telescope, usually at a distance of twice the focal length. In practice, these optical aberrations do not impede the functionality of the telescope, as the 2×2 grid of four 200mm PMTs allows the telescope point spread function, a parameter characterizing the spatial light distribution, to be relaxed. Hence no corrector plate is used in the design.

The telescope utilizes a 1.6m spherical mirror and a octagonal aperture situated at a distance of 1 m from the primary mirror. The aperture sits at a height of 1.24 m and hosts 2×2 grid of four 200mm PMTs. This schematic achieves the set 30° × 30° FOV. Adjusting for the shadow of the aperture along with the camera box containing the PMTs, the telescope still provides the necessary 1 m^2 collecting area. The complete dimensions can be seen in figure 5.

A ray-tracing simulation was employed to study on-axis (blue - figure 6) and off-axis (green - figure 6) optical beams. The results are shown in figure 6. The on-axis beams are of particular importance, as the nature of the 2×2 grid of PMTs is accompanied with a present dead spot in the centre, a point on the camera box where no reflected light could get detected. Furthermore, light detection is problematic even towards the edge of the camera box, as the PMTs do not cover the entire surface of the box.

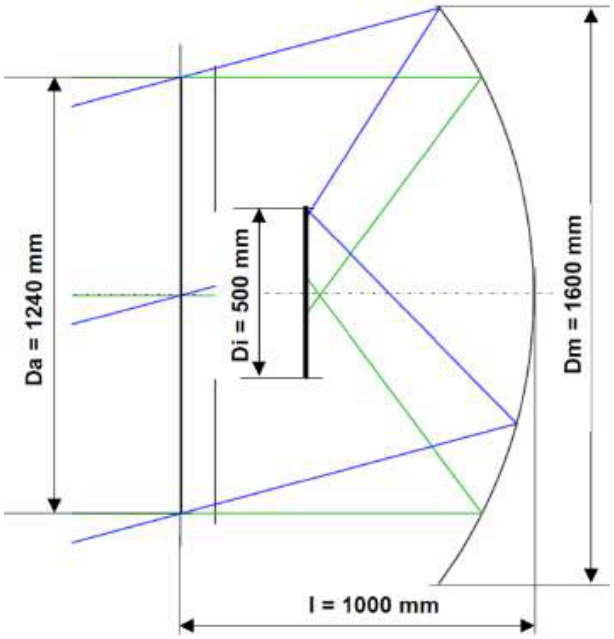

Figure 5 The dimensions of the FAST prototype telescope's optical system. D_a is the face-to-face size of the octagonal telescope aperture, D_i is the side length of the square camera box, D_m is the diameter of the primary mirror, and l is the mirror-aperture distance. Taken from [6]

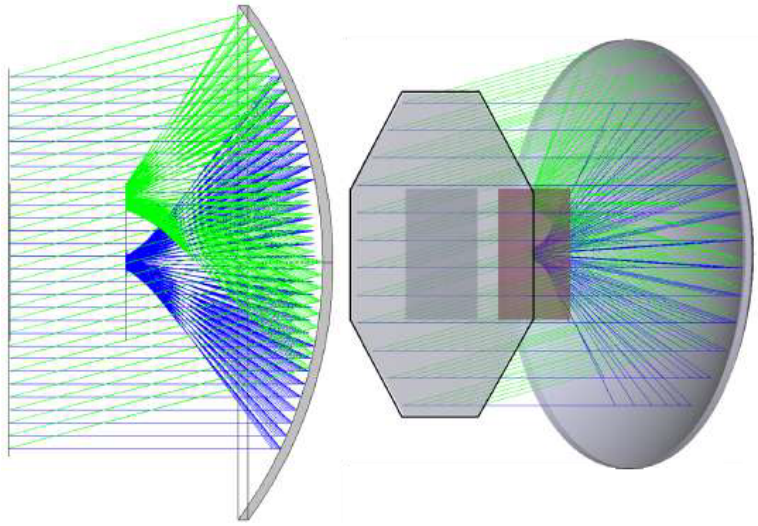

Figure 6 2D (left) and 3D (right) ray-tracing simulation for optical performance of parallel on-axis rays (blue) and off-axis rays (green). [6]

To eliminate a total lack of signal gained from on-axis optical beams several various optical components are utilized. To diminish the signal loss towards camera box edges, a mirror band is installed on the sides of the case. On the very centre of the box, a mirror pyramid along with a diffuser is used to remove the central dead zone of the camera box. The whole camera box can be seen in an example from ray-tracing software simulation in figure 7.

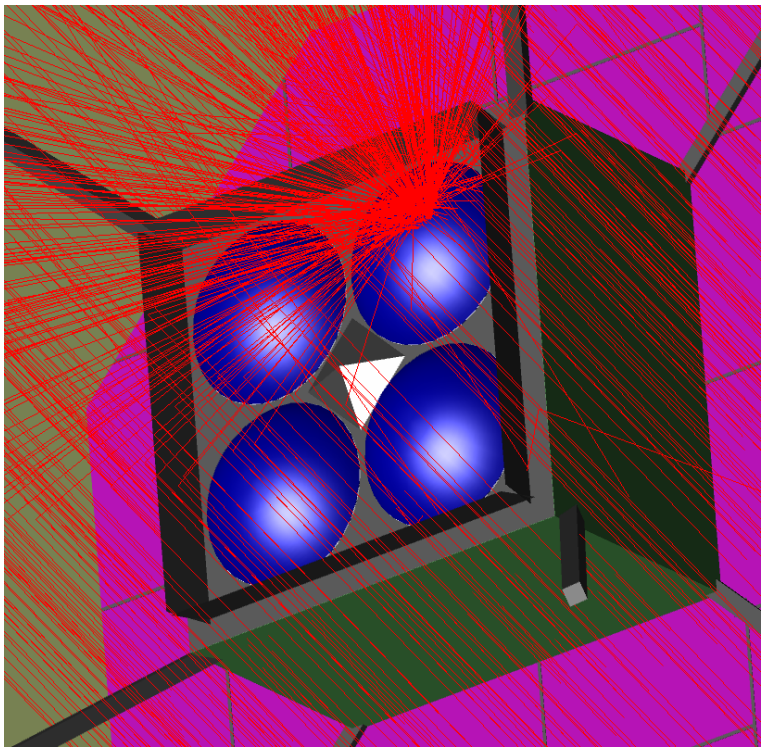

Figure 7 Details of the camera box with four 200mm PMTs from a ray-tracing software simulation. [10]

The simulations previously introduced used a single spherical mirror. This might be the simplest and most elegant solution, however the cost along with the difficulty of transportation of such a large mirror has proven to be too high. Therefore, the FAST telescope uses a segmented primary mirror. Several patterns were designed to conform with the FAST project requirements, primarily the 1 m^2 aperture collecting area. The various shapes of the primary mirror can be seen in figure 8.

The simplest segmented design with the lowest cost is shown in 8(a) with a central circular mirror with 6 circular mirrors surrounding it. This pattern is accompanied with a dead zone between the individual mirrors. This can easily be solved with mirrors overlapping each other, as seen in 8(b). This results in a slightly reduced collective area. The dead spots however have shown to still be too large, minimizing the effective reflective area. Reduction of the dead zones can be achieved by cutting the mirrors, as shown in 8(c). Nevertheless, the optimal design is a central circular mirror surrounded with 8 "petal" shaped side mirrors. This configuration offers a total reflective area of 2.39 m^2. The final shape can be seen in 8(d).

The mirrors themselves are produced by the Joint Laboratory of Optics of the Palacky University and the Institute of Physics of the Academy of Sciences of the Czech Republic. Custom-made borosilicate glass substrate offers ideal mechanical properties. The mirror surface is coated with layers of Al and SiO_2. These layers provide sufficient reflectivity in the given fluorescent UV spectral range of 300 nm - 420 nm. The spectral reflectance is shown in figure 9.

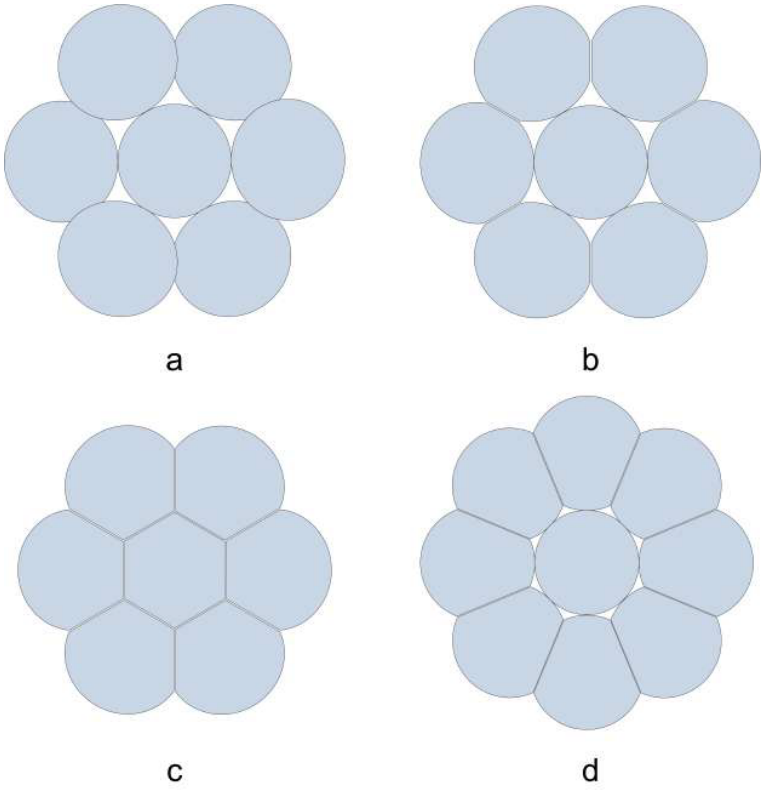

Figure 8 | Fast telescope segmented primary mirror designs. [6]

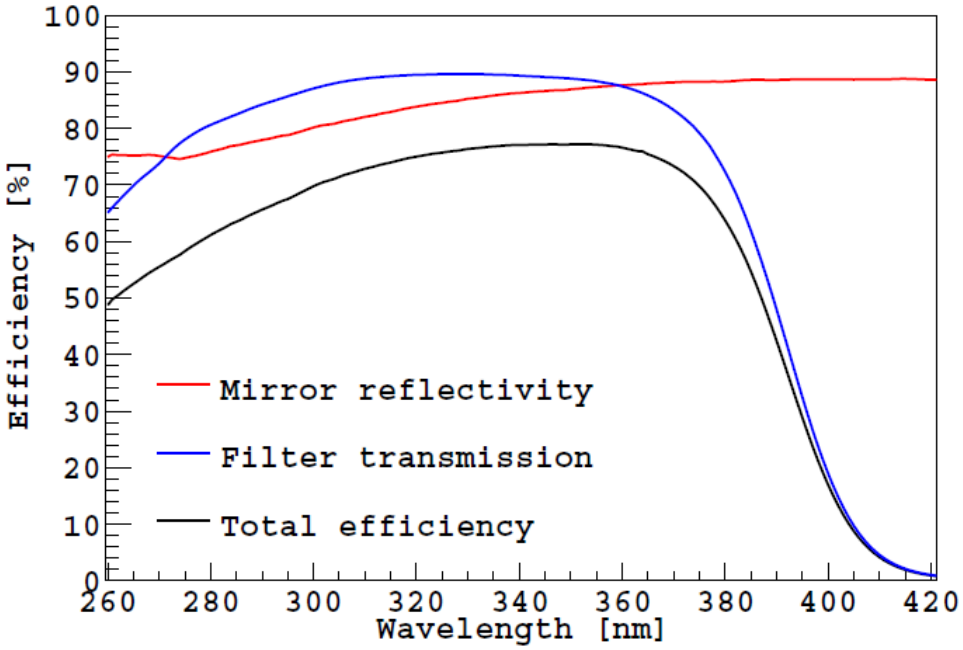

Figure 9 Spectral reflectivity of the FAST telescope mirror (red) along with UV filter transmittance (blue). [6]

A UV filter is utilized to further reduce the exposure to parasitic night-sky background light. A ZWB3 filter manufactured by Shijiazhuang Zeyuan Optics is installed at the aperture of the telescope. The spectral transmissivity in the UV portion of electromagnetic radiation is shown in figure 9. The maximum light incidence angle for this specific setup is $\sim 15°$. The losses of such design are negligible compared to a setup where the filter is located on the camera box. Additionally, a window would have to be used in the filter's place to protect the telescope against dust sedimentation and winds. The entire filter is constructed in a number of segments to fit the octagonal shape of the aperture of the FAST telescope.

The mechanical structure of the telescope is built from commercially available aluminum profiles. The light weight of such support system allows easy transportation along with simple installation. Furthermore, the aluminum profiles provide a stable platform for the FAST optics. The framework offers a single degree of freedom to modify the elevation of the telescope to discrete values of 0°, 15°, 30° and 45°. The structure is covered with a gray shroud to eliminate the effects of the environment and to protect the optical components from parasitic night-sky background light.

Figure 10 | A FAST telescope prototype. [6]

1.5. Photomultiplier Tubes

Photomultiplier tubes detect light by employing the external photoeletric effect. Incoming light passes through the input window. Upon interacting with the material of a photocathode, electrons are emitted from atoms and are further sped up and focused onto a first dynode. There, secondary emission of electrons occurs and subsequent electrons are likewise accelerated and focused towards further dynodes, occasionally called electron multipliers. Afterwards, the multiplied electrons are gathered and detected by an anode on the tip of the PMT.

FAST telescope uses a PMT produced by Hamamatsu (mod. R5912-03). This commercially available PMT offers adequate optical and electrical quality for the purpose of measuring faint fluorescent UV radiation produced by an EAS. Its spectral response ranges from 300 nm to 650 nm, well within criteria of the FAST project for detecting photons produced by deexcitation of nitrogen atoms in Earth's atmosphere. The tube of PMT measures $\sim$ 200 mm. The input window is manufactured from borosilicate glass, offering great transmittance of UV light, as shown in figure 12. The interior of the PMT is constructed from a bialkali photocathode along with 10 box and linear-focused dynode stages. [11]

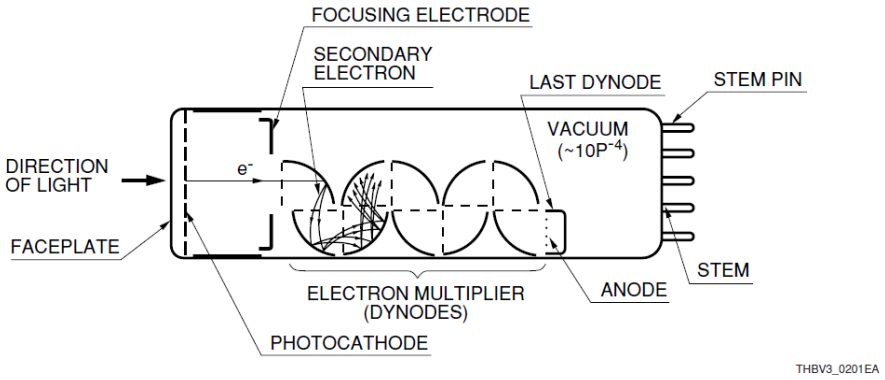

Figure 11 | A schematic of a typical Photomultiplier Tube. [11]

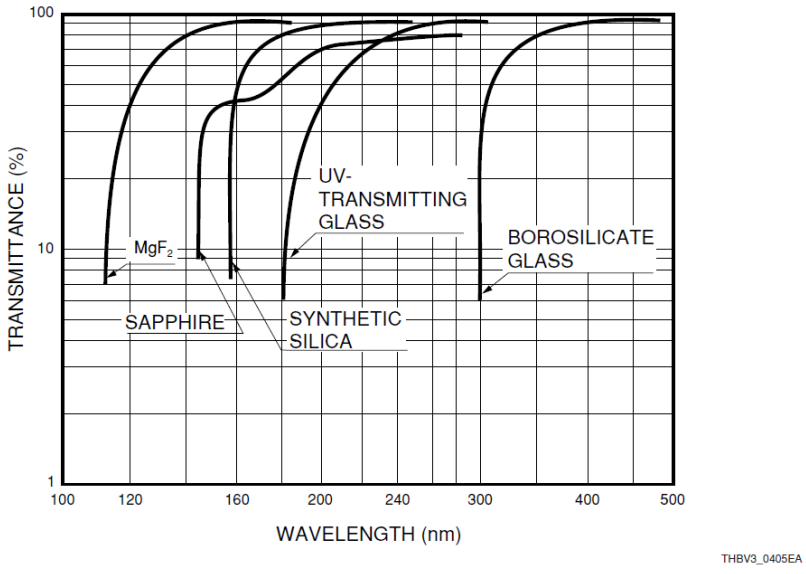

Figure 12 | Spectral characteristics of input window materials of Hamamatsu PMTs. Borosilicate glass is of particular importance as the PMTs on FAST telescopes utilize a window of the aforesaid material. [11]

1.5.1. Time dependency

Fluctuations and general instability can be seen over various and diverse amount of time. Variations over short time intervals are called time drift and variation over a long time interval, generally more than $\sim 10^3$ hours is called time characteristic. An example of such time drift properties is shown in figure 13.

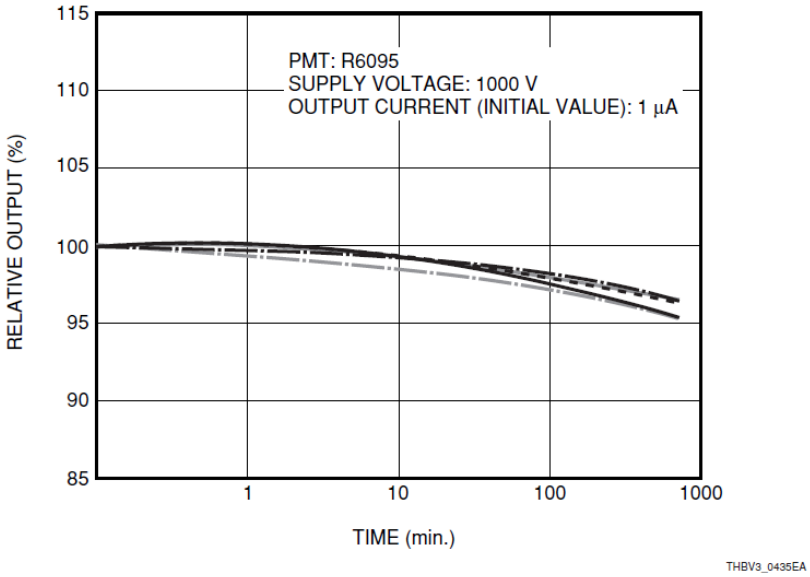

Figure 13 | An example of time drift characteristics. [11]

Significant signal loss can only be measured after minutes of run time of a given PMT. Such time interval is way longer than the regular measurement of analysed calibration runs. Details about the calibration measurements can be found in Section 1.6.2. Furthermore, the signal loss due to time drift hypothetically measured would reflect only in absolute numbers. By comparing the individual PMTs on a single FAST telescope, the relative values should in theory stay stabilized.

Lacking any information about the life characteristic of the module employed on the FAST telescope, no reasonable assumption can be made about the behaviour of PMT signal after a large period of time. However, as was the case with time drift, in theory all four PMTs experience the same conditions and thus should show the same signal loss or signal gain after any amount of time. The difference could be noticeable in absolute numbers, nevertheless in relative values the signal should stay stabilized. Data analysis on such time characteristic behaviour can be found in Section 2.6.

1.5.2. Temperature dependency

In precise measurements for low-light-level optical applications temperature stability has to be guaranteed as the sensitivity of PMTs to ambient temperature is rather significant. If no temperature regulation can be secured, calibration and other comparative methods could be employed to diminish the effects of temperature discrepancy.

Analysis of two aspects of temperature dependency are provided by the manufacturer. A relation between cathode sensitivity and wavelength of incoming light is shown in figure 14. In practice no sensitivity signal variations are present as the bialkali photocathodes operate in a stable manner for the photons of UV portion of the electromagnetic spectrum produced by UHECRs. The wavelength of such radiation is within the range of 300 nm to 420 nm.

Temperature variations have essentially no effect on dynode photoelectron gain and therefore any such influence can be disregarded.

However, low temperatures have drastic impact on saturation current of bialkali photocathodes. Increase of the photocathode surface resistance may induce a loss of signal output linearity in regards to the incident light, a saturation effect for the photocathode. Such relation is shown in figure 15. Nevertheless, the temperature fluctuations affect all four PMTs equally, thus the signal

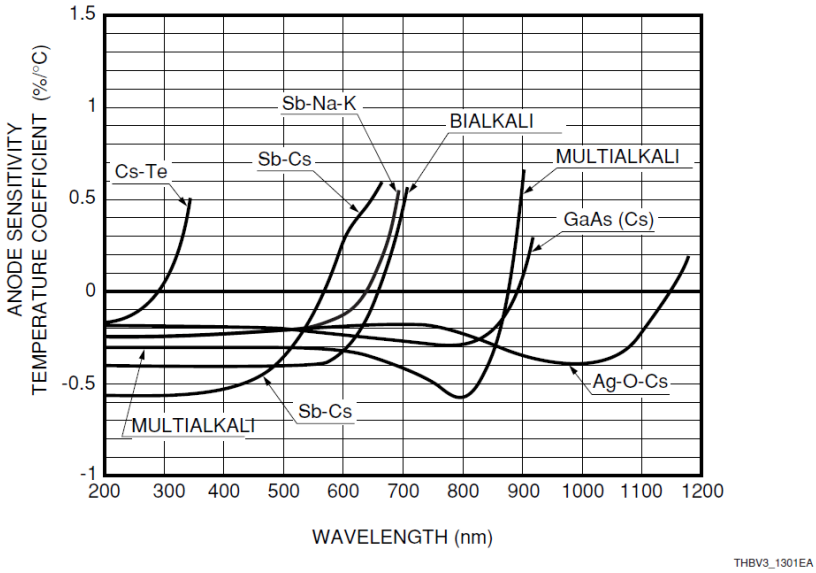

Figure 14 A characteristic describing relation between anode sensitivity and wavelength of the incident light. Bialkali relation is of particular importance as the photocathodes of PMTs on FAST telescopes utilize said material. [11]

variations should only be noticeable in absolute numbers. By comparing the individual PMTs on a single FAST telescope, the relative values should in theory stay stabilized.

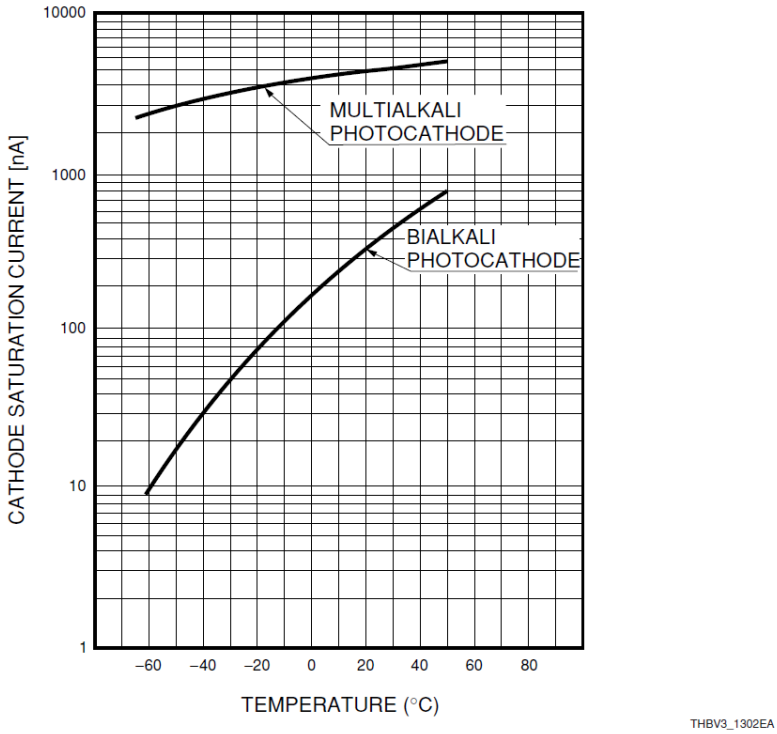

Figure 15 A characteristic describing relation between saturation current and temperature. Bialkali relation is of particular importance as the photocathodes of PMTs on FAST telescopes utilize said material. [11]

1.6. Data acquisition

The entire FAST telescope electronics chain consists of commercially available components. The 2×2 grid of the camera box is comprised of four 200mm PMTs (mod. R5912-03, Hamamatsu) and an AC-coupled active base (mod. E7694-01, Hamamatsu) with maximum operational voltage of $\sim$ 2600 V. High voltage is delivered by a NIM-mounted module (mod. N1470, CAEN), with signal from the base travelling through a low-pass (LP) filter (mod. CLPFL-0015, Crystek) to eradicate noise with frequency higher than 15 Mhz. The signal is then run through an amplifier (mod. 777, Phillips Scientific). A fast analog-to-digital converter (FADC, mod. SIS3316, Struck Innovative Systeme) is situated in a VME crate along with a GPS module (mod. GPS2092, Hytec) and a single-board PC (mod. V97865, GE Intelligent platforms) which operates the Data Acquisition (DAQ) software. A schematic of the electronics chain can be seen in figure 16.

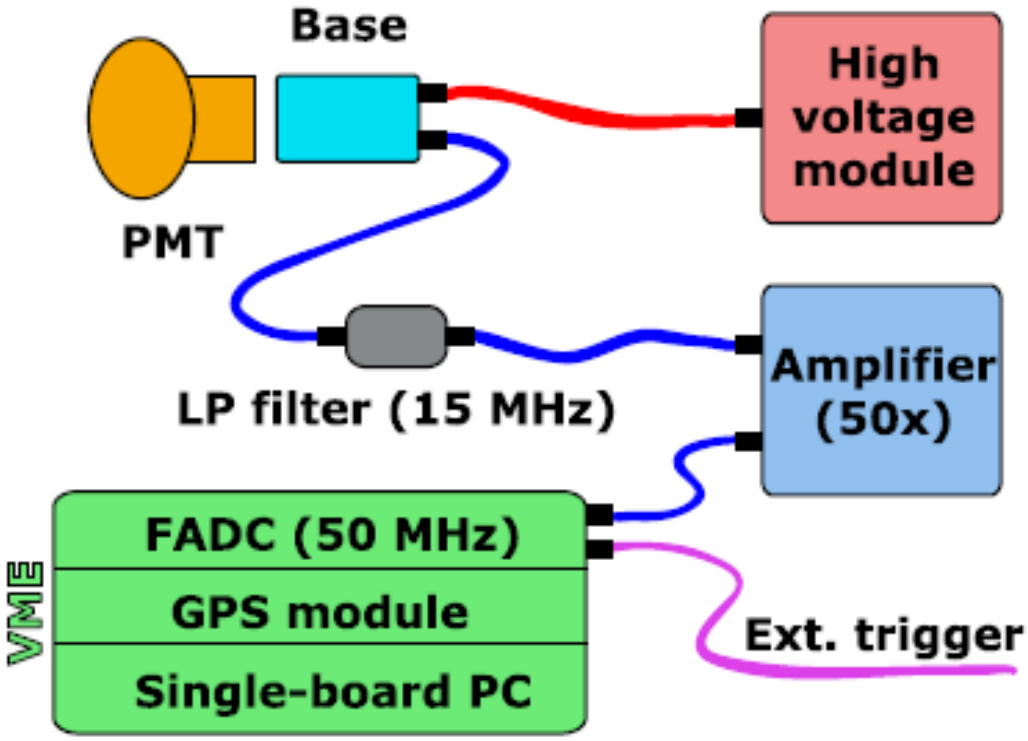

Figure 16 | A PMT electronics chain of a FAST telescope. [7]

1.6.1. Environmental conditions

The FAST telescope is equipped with an environmental conditions monitoring system. Several temperature sensors (mod. DS18B20+, Dallas) are present to monitor both indoor and outdoor temperature and additionally the temperature of the rack case. The same sensor is also present on the FAST camera box, however in a waterproof case. A combined sensor of temperature, humidity and pressure (mod. BME280, Bosch) is situated on the aluminum profile supporting the telescope optics. A shutter sensor is located near the entrance. The readout system is based on a Raspberry Pi 4 (RPi4) computer. Further detail on the FAST conditions monitoring system is provided in Section 2.1.1

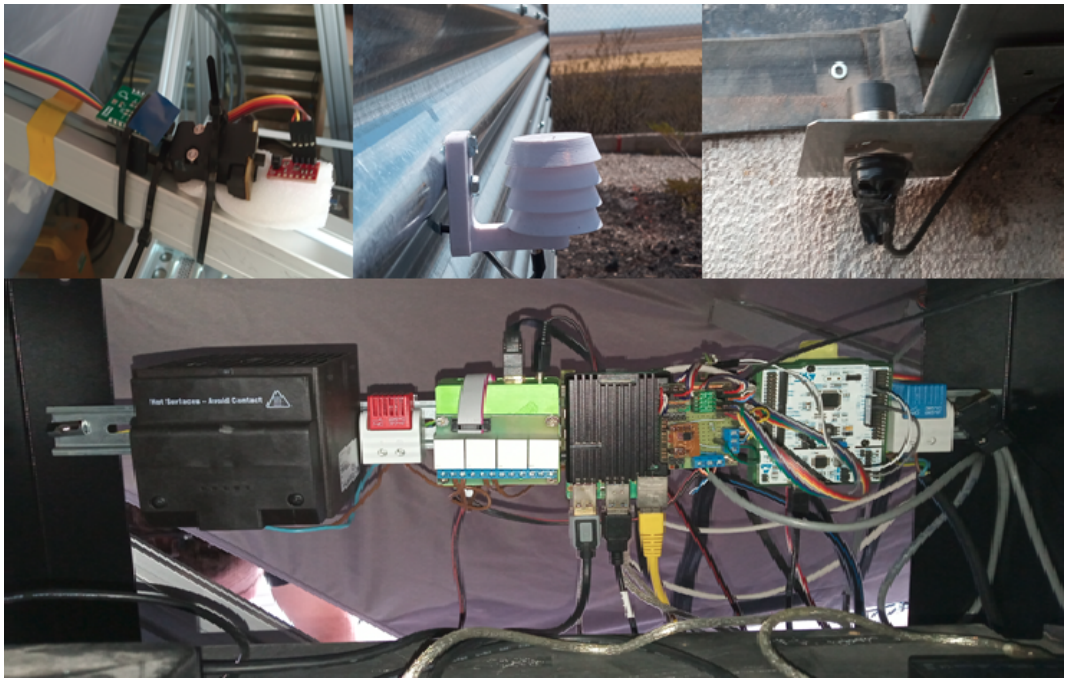

Figure 17 Sensor photos and their location. An indoor Dallas temperature sensor with a Bosh combined sensor (top left), outdoor Dallas temperature (top centre), shutter sensor (top right) and the electronics chain including the RPi4 computer and a Dallas rack case temperature sensor (bottom) can be seen. Taken from an internal presentation of the FAST collaboration.

1.6.2. Calibration

For proper functionality calibration of the four 200mm PMTs is mandatory. A series of one-photon laboratory measurements occurred in 2020 to find a relation between the gain of the PMT and its voltage level. For a selected high voltage range measurement a fit was performed. A calibration constant can be obtained from the fit. The original idea was to set up the same gain for all PMTs, but some showed higher or lower spectral responses. For that reason each PMT bears its own calibration constant. Moreover, recalculation of the constants is essential after certain amount of time, as its value is not completely fixed in time. The calibration was performed for both TA and PAO sites. Values of all four calibration constants can be seen in figure 23.

At the PAO site a UV LED flasher (RLT365-10E) is permanently installed onto one of the FAST telescopes. It provides UV radiation with peak wavelength of 365 nm at 25 °C with operating temperature range from -30 °C to +85 °C [12]. Dedicated UV LED measurements are performed at the beginning and end of each observation run. The operation of the UV LED flasher is done through a microcontroller (STM32F411). The UV LED signal varies as it not equipped with any temperature stabilization. The temperature difference results in a shift of emitted spectrum of the UV LED light source. The effects of ambient temperature can see been in figure 18.

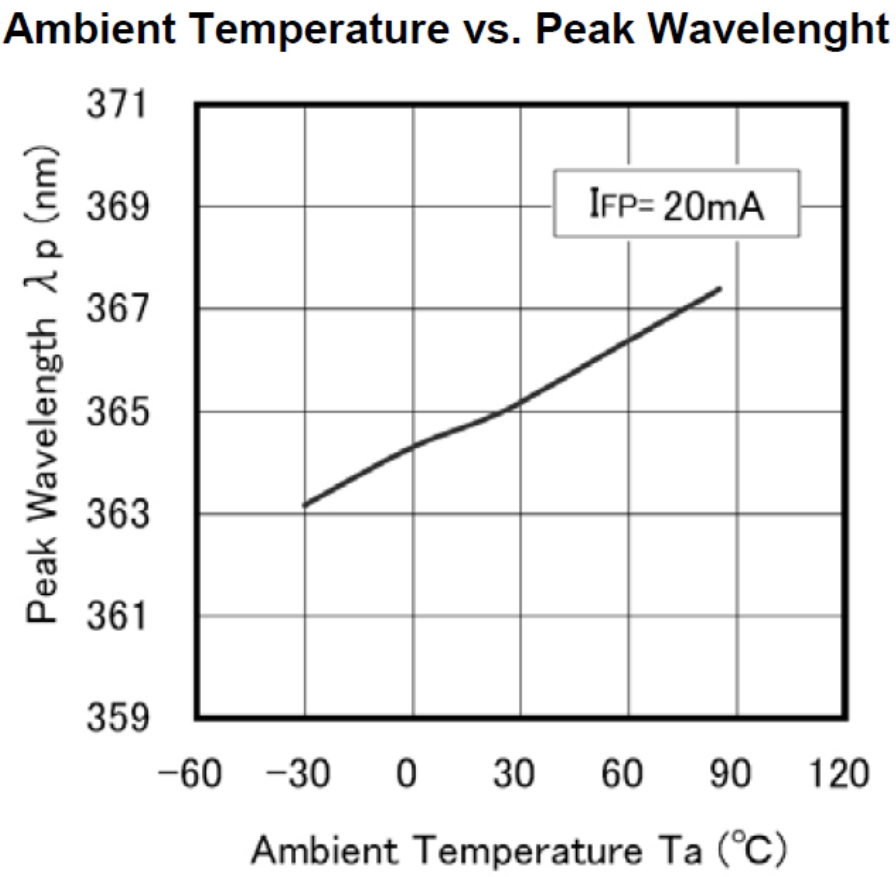

Figure 18 | Relation between ambient temperature and the wavelength of UV light emitted by the UV LED flasher. [12]

Temperature fluctuations of the UV LED flasher shift the wavelength of light it emits onto the PMTs. This may result in a change of the efficiency of the PMT, as transmittance of the borosilicate glass that the input windows is manufactured from exhibits a degree of wavelength dependency. Furthermore, saturation current of the bialkali photocathodes is heavily dependant on ambient temperature. These relations can be seen in figures 12 and 15, respectively. Such effect shall however only be noticeable in absolute numbers. The alteration of transmittance and saturation current should, in theory, affect all four PMTs equally. By comparing the individual PMTs on a single FAST telescope, the relative values should in theory stay stabilized.

The stability of such process has shown potential in relative calibration. Comparing the signal of all four PMTs on a single telescope can provide information regarding the status of individual PMTs and their reliability. Such procedure can yield valuable data regarding their temperature stability, time stability and quality or material deterioration. For the purpose of this thesis, only calibration data from the PAO site in Argentina shall be examined.

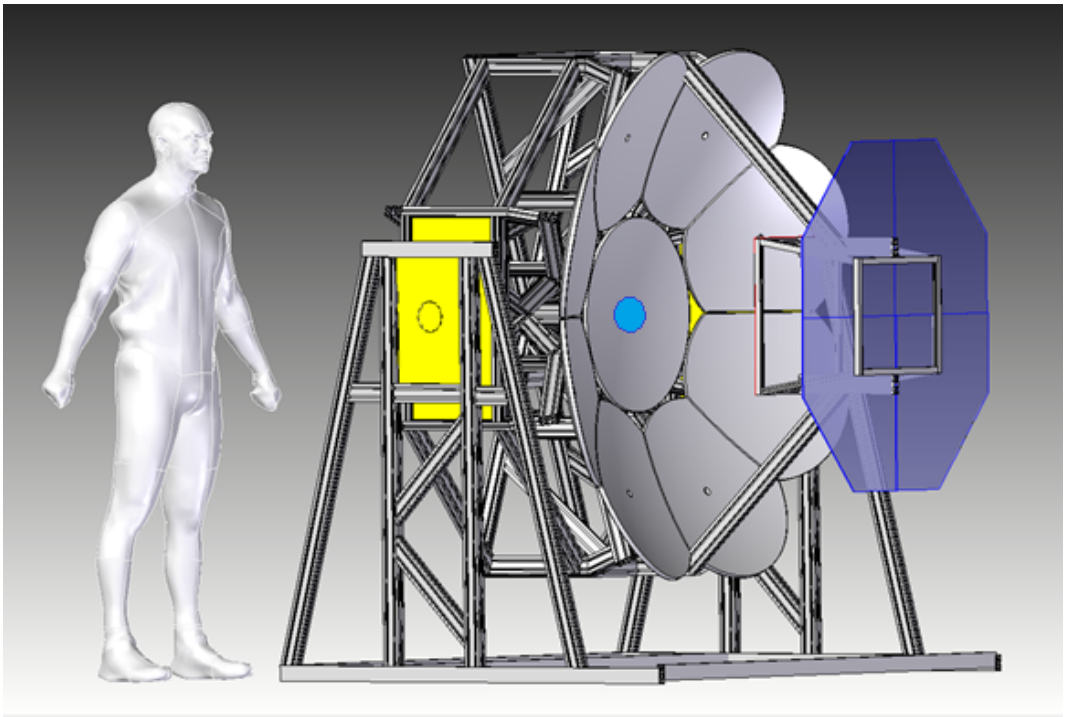

Figure 19 Location of the UV LED flasher (blue dot) on a central circular mirror of the FAST telescope. Edited from [8].

Figure 20 Photos from various angles of the UV LED flasher used in calibration measurements.

2. Data Analysis

2.1. PAO database

For the purpose of data storage and their subsequent analysis a database has been established on a MariaDB server in Joint Laboratory of Optics of the Palacky University, Czech republic. For the purpose of this thesis a guest account was created to ensure proper access. For database viewing, a free multi-platform database program DBeaver[13] was utilized. The program offered sufficient graphical interface to properly assess individual tables of the database.

The database contains measurements from both Telescope Array, Utah - USA and Pierre Auger Observatory, Argentina. This thesis however only examines data from the PAO site and therefore only such data is to be reviewed.

The database consists of several tables with measurements of various data. Three of those tables contain instrumental data for proper calibration analysis and shall be listed here.

- TelescopeConditions - A table containing various data about the conditions of the FAST telescope.
- UVLEDTab - A table containing information about the UV LED calibration measurements.
- AbsCalibTab - A table containing data about the calibration constants described in Section 1.6.2.

2.1.1. Telescope Conditions

This table contains data about the individual conditions of the telescope as measured by the many sensors surrounding it. The sheet provides information of particular importance on:

- timestamp - Details of the specific time the measurement occurred. The information is indexed in Epoch Time, the number of seconds that have elapsed since the midnight (UTC time) of January 1st, 1970. For the conversion into a more ordinary format an Epoch Time converter can be used.
- temprack - Temperature measurements of a rack case in the FAST hut. Measured in °C.
- tempout - Outdoor temperature measurements. Measured in °C.
- tempin - Inside temperature measurements. Measured in °C.
- tempcam - Camera temperature measurements. This temperature sensor is located the closest to the four PMTs and these values will be used in the calibration analysis. Measured in °C.
- tempin2 - Secondary inside temperature measurements. Measured in °C.
- shutterClosed - Information about the shutter being closed. If the value equals to 0, the shutter is opened and if the value equals to 1, the shutter is closed. All the UV LED measurements were conducted with shutter closed to eliminate parasitic environmental background light.

	id	timestamp	fastid	temprack	tempvme	tempnim	tempout	tempin1	tempcam	tempin2	humidity	pressure	shutterClosed	lightIn	lightOut
48771	48,820	1,582,836,216	4	32.375	32.75	32.188	29.438	33.375	35.812	33.304	14.408	858.802	1	0.43	2,485.76
48772	48,821	1,582,836,310	4	32.312	32.688	32.125	29.5	33.252	35.75	33.208	14.366	858.813	1	0.43	2,780.16
48773	48,822	1,582,836,402	4	32.188	32.562	32.062	29.375	33.188	35.688	33.08	14.503	858.812	1	0.43	2,840.32
48774	48,823	1,582,836,492	4	32.125	32.562	32	29.375	33.125	35.562	33.014	14.522	858.781	1	0.43	2,781.44
48775	48,824	1,582,836,582	4	32.062	32.438	31.938	29.688	33.062	35.5	32.968	14.482	858.748	1	0.43	2,693.12
48776	48,825	1,582,836,674	4	32	32.375	31.875	29.625	33	35.438	32.897	14.611	858.766	1	0.42	2,650.88
48777	48,826	1,582,836,763	4	31.875	32.252	31.753	29.875	32.875	35.312	32.852	14.572	858.872	1	0.43	2,396.8
48778	48,827	1,582,836,855	4	31.875	32.188	31.688	29.688	32.875	35.252	32.816	14.516	858.825	1	0.42	2,279.04
48779	48,828	1,582,836,943	4	31.812	32.125	31.688	29.75	32.812	35.188	32.76	14.655	858.918	1	0.42	2,206.08
48780	48,829	1,582,837,036	4	31.75	32.125	31.625	29.438	32.75	35.125	32.674	14.659	858.832	1	0.43	2,138.88
48781	48,830	1,582,837,126	4	31.688	32.062	31.562	29.625	32.688	35	32.623	14.599	858.876	1	0.42	2,120.32
48782	48,831	1,582,837,218	4	31.625	31.938	31.562	29.438	32.625	34.938	32.541	14.681	858.824	1	0.43	2,142.08
48783	48,832	1,582,837,310	4	31.562	31.875	31.5	29.312	32.562	34.875	32.46	14.737	858.911	1	0.42	2,159.36
48784	48,833	1,582,837,399	4	31.562	31.875	31.438	29.312	32.5	34.752	32.399	14.782	858.858	1	0.42	2,153.6
48785	48,834	1,582,837,488	4	31.562	31.812	31.375	29.25	32.438	34.688	32.333	14.853	858.91	1	0.42	2,119.04
48786	48,835	1,582,837,578	4	31.438	31.753	31.312	29.25	32.375	34.625	32.318	14.885	858.834	1	0.43	2,058.88
48787	48,836	1,582,837,668	4	31.438	31.75	31.253	29.125	32.312	34.562	32.246	14.873	858.851	1	0.42	2,001.92
48788	48,837	1,582,837,759	4	31.375	31.688	31.25	29.062	32.25	34.5	32.17	15.064	858.861	1	0.42	1,904
48789	48,838	1,582,837,849	4	31.312	31.625	31.188	29.062	32.188	34.375	32.079	15.089	858.879	1	0.41	1,808
48790	48,839	1,582,837,939	4	31.312	31.562	31.125	28.938	32.125	34.312	32.007	15.207	858.813	1	0.42	1,794.56
48791	48,840	1,582,838,028	4	31.188	31.562	31.062	28.875	32.062	34.188	31.941	15.304	858.865	1	0.42	1,801.6
48792	48,841	1,582,838,117	4	31.188	31.438	31.062	28.812	31.938	34.125	31.834	15.392	858.862	1	0.41	1,845.76

Figure 21 An example screenshot of the TelescopeConditions table in the PAO FAST database.

2.1.2. UV LED table

This table contains data on the individual UV LED measurements that were analysed. The sheet provides information of particular importance on:

- timestamp - Details of the specific time the measurement occurred. The information is indexed in Epoch Time, the number of seconds that have elapsed since the midnight (UTC time) of January 1st, 1970. For the conversion into a more ordinary format an Epoch Time converter can be used.
- chanid - An ID of a channel marking specific PMTs. Channel 0-3 correspond with the four 200mm PMTs present at the camera box of each FAST telescope.
- counts - Counts of PMT events measured by the telescope instrument. In correlation with the calibration constants, this data will yield final signal values in the number of photo-electrons(Np.e).
- stdev - Standard deviation of count measurements for each PMT.

	timestamp	chanid	counts	stdev	gpstime	sampletabid
3948	1,600,401,947	3	719.171	3.629	0	1,600,401,947
3949	1,600,401,957	0	965.167	4.72	0	1,600,401,957
3950	1,600,401,957	1	634.824	3.147	0	1,600,401,957
3951	1,600,401,957	2	816.377	4.011	0	1,600,401,957
3952	1,600,401,957	3	719.851	3.589	0	1,600,401,957
3953	1,600,401,967	0	965.292	4.701	0	1,600,401,967
3954	1,600,401,967	1	634.856	3.155	0	1,600,401,967
3955	1,600,401,967	2	816.304	3.991	0	1,600,401,967
3956	1,600,401,967	3	719.769	3.577	0	1,600,401,967
3957	1,600,420,425	0	952.142	4.816	0	1,600,420,425
3958	1,600,420,425	1	630.928	3.213	0	1,600,420,425
3959	1,600,420,425	2	783.852	3.996	0	1,600,420,425
3960	1,600,420,425	3	723.951	3.73	0	1,600,420,425
3961	1,600,420,435	0	951.644	4.842	0	1,600,420,435
3962	1,600,420,435	1	631.591	3.199	0	1,600,420,435
3963	1,600,420,435	2	784.355	4.045	0	1,600,420,435
3964	1,600,420,435	3	724.505	3.772	0	1,600,420,435
3965	1,600,420,445	0	951.695	4.812	0	1,600,420,445
3966	1,600,420,445	1	631.974	3.179	0	1,600,420,445
3967	1,600,420,445	2	787.485	3.999	0	1,600,420,445
3968	1,600,420,445	3	725.781	3.756	0	1,600,420,445
3969	1,600,420,455	0	947.128	4.857	0	1,600,420,455
3970	1,600,420,455	1	629.598	3.186	0	1,600,420,455

Figure 22 | An example screenshot of the UVLEDtab table in the PAO FAST database.

2.1.3. Calibration table

This table contains data on the specific calibration constants corresponding to their respective PMTs. The sheet provides information of particular importance on:

- timestamp - Details of the specific time the measurement occurred. The information is indexed in Epoch Time, the number of seconds that have elapsed since the midnight (UTC time) of January 1st, 1970. For the conversion into a more ordinary format an Epoch Time converter can be used.
- chanid - An ID of a channel marking specific PMTs. Channel 0-3 correspond with the four 200mm PMTs present at the camera box of each FAST telescope.
- value - Individual values of the calibration constant corresponding to respective channel IDs, ergo to the four PMTs.

	timestamp	chanid	value
1	1,555,027,013	0	7.909
2	1,555,027,013	1	8.122
3	1,555,027,013	2	8.212
4	1,555,027,013	3	8.018
5	1,555,407,312	0	5.728
6	1,555,407,312	2	4.427
7	1,555,407,312	3	21.815

Figure 23 | An example screenshot of the AbsCalibTab table in the PAO FAST database.

Note that more calibration constants are provided in the database. For the purpose of data analysis in this thesis, only the most recent values are utilized as they are the most accurate in reporting the actual signal value of the PMT.

2.2. Software

For any subsequent data analysis Python programming language[14] was utilized. An integrated development environment of Pycharm[15] developed by Jetbrains was also used. For proper data management, operation and visualization NumPy[16], MatPlotLib[17] and SQLAlchemy[18] modules were utilized. NumPy offers comprehensive mathematical and data processing functions for the Python programming language instrumental to the analysis. For visualizations and data plotting MatPlotLib was employed. This module offers excellent graphical framework for proper static graphic images for Python. As all the calibration and FAST telescope conditions data was stored on a SQL database on a MariaDB server in Joint Laboratory of Optics of the Palacky University, Czech republic, an SQL toolkit and object relational mapper had to be utilized. Python SQLAlchemy library provided exactly that, an SQL open-source toolkit for database interaction. Python scripts produced for the calibration data analysis are stored on the CD attached to the thesis.

2.3. Signal shape

The UV LED calibration measurements occur with closed shutter with minimal parasitic environmental background electromagnetic radiation. The individual flashes of the diode last for $\sim$ 1000 ns (1 μm). An example of the shape of such calibration signal is shown in figure 24. The UV LED calibration cycle contains five such flashes, with an interval of $\sim$ 10 s between individual flashes. Per UV LED cycle, five signals are obtained per PMT, for a total of 20 data points.

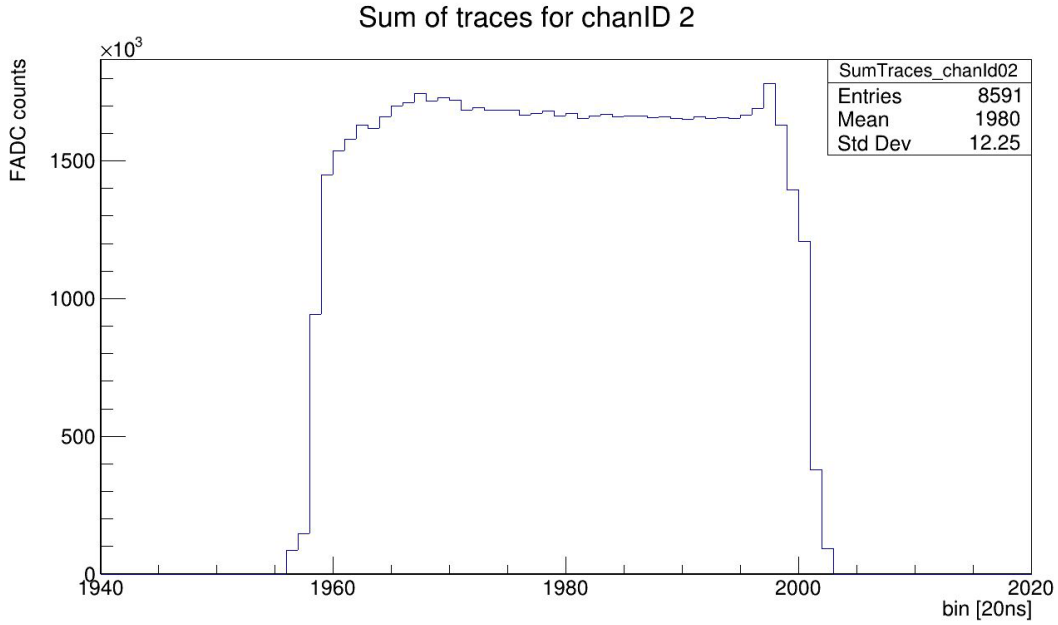

Figure 24 An example shape of the UV LED calibration measurement signal from a FAST telescope. Taken from an internal presentation of the FAST collaboration.

For practical purposes a single value is obtained from the complete signal shape as seen in figure 24. A projection of sum of the bin traces is generated to find the most probable (most frequent) FADC amplitude. The process can be seen in figure 25. Counts, as seen in the PAO UVLEDtab database in figure 22 are already calculated from such procedure. Any further analysis has been done on these values, the most probable FADC amplitude from a single UV flash.

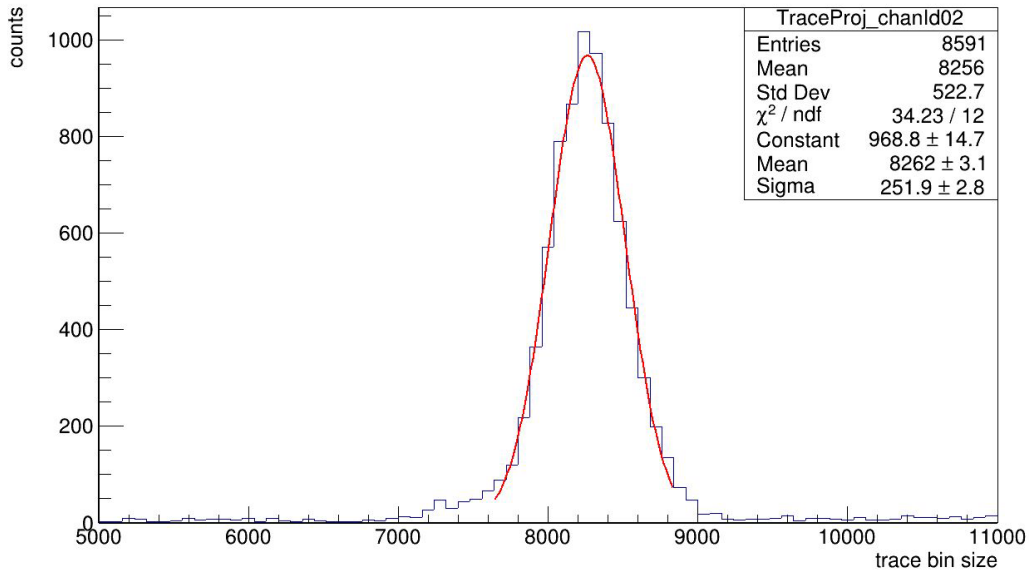

Figure 25 An example of the UV LED calibration sum traces and obtainment of a value from a single signal. Taken from an internal presentation of the FAST collaboration.

2.4. Example run

A single UV LED calibration run contains 5 UV flashes. FAST telescope is equipped with four 200mm PMTs, in total from a single calibration run 20 data points are obtained. Relative signal values can be obtained by comparing the signal of all PMTs to a single reference PMT. PMT 1 was chosen as the reference and all subsequent data analysis will be done with the identical reference PMT. The relative values are calculated by dividing the signal value of individual PMTs by the signal value of a reference PMT, in this case PMT 1. By such procedure from a single UV calibration run, 20 dimensionless values are gained. An example run of such method is seen in figure 26.

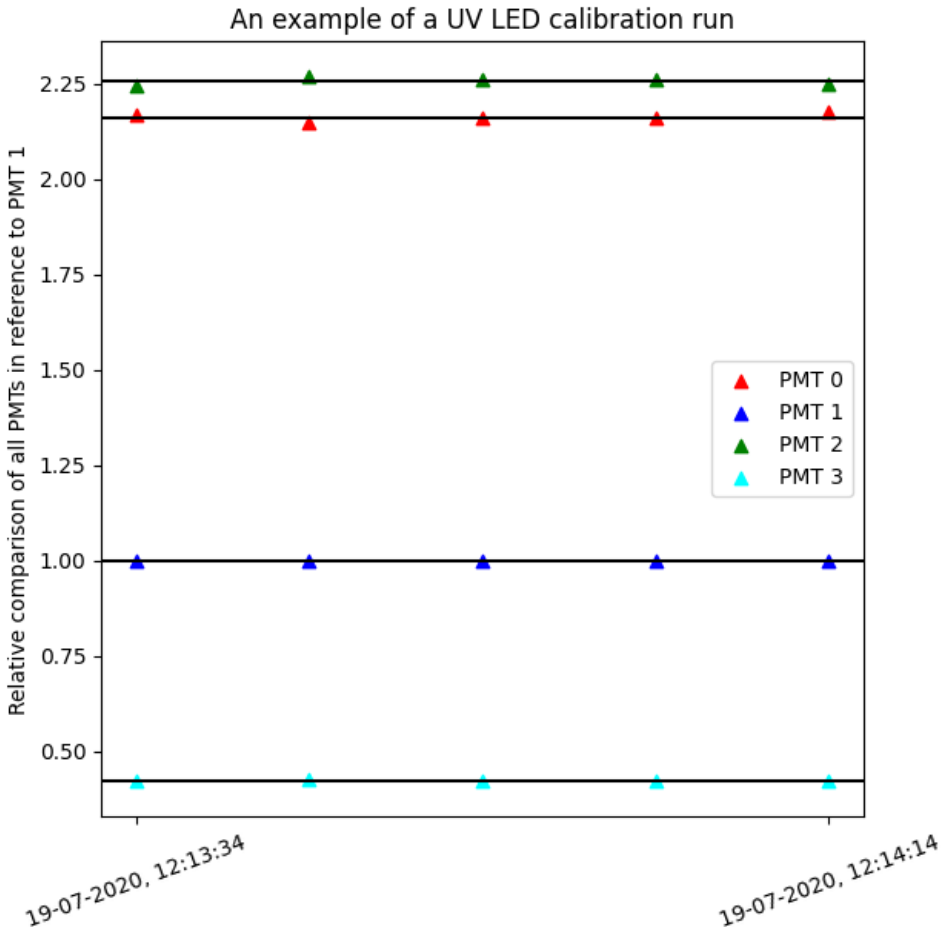

Figure 26 | An example of a UV LED calibration run.

The absolute values seen in figure 26 are not of any particular significance. The discrepancy of relative signal values is caused by diverse spectral responses of individual PMTs as described in Section 1.6.2. In theory, all PMTs should stay stable (with respect to time in this case), as all four PMTs should respond to the UV LED flash in an equal manner. The values of each PMT should stay equal with respect to time. The absolute numbers may differ, but no shift in the values should be observed, ideally. The black line present at each PMT is at a location of the mean average for the specific signal.

Note that PMT 1 exhibits a relative value of 1, which is only logical as each PMT 1 signal value was divided by itself. In addition, during this specific calibration measurement PMT 3 demonstrates a degree of time stability. Both PMT 0 and PMT 2 show noticeable variance with respect to time. A single UV LED calibration run lasts for $\sim$ 50 s, with 5 flashes with $\sim$ 10 second intervals between them. A screenshot of a Python script that produced figure 26 can be seen in figure 27 and 28. Rough description of the script is provided in the screenshots.

```python
def get_calib_const(calib_type, chanid, ts):  # Defining a function to obtain the calibration constants
    data = {}
    if calib_type == "abs":
        query = sql.select([abscalibtab]).where(abscalibtab.columns.chanid == chanid)
    elif calib_type == "uvled":
        query = sql.select([uvledcalibtab]).where(uvledcalibtab.columns.chanid == chanid)
    else: return 0
    ResultProxy = conn_pao_calib.execute(query)
    res = ResultProxy.fetchall()
    for r in res: data[r[0]] = r[2]
    return data[ts] if ts in data else data[min(data.keys(), key=lambda k: abs(k - ts))]


timestamp_calib_const = 1595335842
calib_const_id0 = get_calib_const("abs", 0, timestamp_calib_const)
calib_const_id1 = get_calib_const("abs", 1, timestamp_calib_const)
calib_const_id2 = get_calib_const("abs", 2, timestamp_calib_const)
calib_const_id3 = get_calib_const("abs", 3, timestamp_calib_const)  # Defining the calibration constants for each PMT

ts = 1595153614  # Timestamp of the selected UV LED calibration run
signal = sql.select([uvledtab]).where(uvledtab.columns.timestamp >= ts).where(uvledtab.columns.timestamp <= ts + 50)
ResultProxy_signal = conn_pao_run.execute(signal)
rows_signal = ResultProxy_signal.fetchall()  # Importing data from the FAST database

y0 = []
y1 = []
y2 = []
y3 = []
time_list = []
while len(time_list) < 5:
    for row in rows_signal:
        if row[1] == 0:
            y0.append(row[2] / calib_const_id0)
            time_list.append(row[0])
        elif row[1] == 1:
            y1.append(row[2] / calib_const_id1)
        elif row[1] == 2:
            y2.append(row[2] / calib_const_id2)
        elif row[1] == 3:
            y3.append(row[2] / calib_const_id3)  # Creating data lists for all PMT signal values
```

Figure 27 | A first example of the Python Script that produced figure 26.

```python
y0_relative = np.divide(y0, y1)
y1_relative = np.divide(y1, y1)
y2_relative = np.divide(y2, y1)
y3_relative = np.divide(y3, y1)  # Taking their relative values in reference to PMT 1

date = []
for timestamp in time_list:  # Converting timestamp into a suitable format
    date.append(time.strftime('%d-%m-%Y, %H:%M:%S', time.localtime(timestamp)))

values = [{'name': 'PMT 0', 'x': time_list,
           'y': y0_relative, 'color': 'r', 'marker': '^'},
          {'name': 'PMT 1', 'x': time_list,
           'y': y1_relative, 'color': 'b', 'marker': '^'},
          {'name': 'PMT 2', 'x': time_list,
           'y': y2_relative, 'color': 'g', 'marker': '^'},
          {'name': 'PMT 3', 'x': time_list,
           'y': y3_relative, 'color': 'cyan', 'marker': '^'}]

for signal in values:
    plt.scatter(signal['x'], signal['y'],
                color=signal['color'],
                label=signal['name'],
                marker=signal['marker'])
plt.legend()
plt.xlabel("Date")
plt.xticks([time_list[0], time_list[4]],
           [date[0], date[4]], rotation=20)
plt.axhline(np.average(y0_relative), color="black")
plt.axhline(np.average(y1_relative), color="black")
plt.axhline(np.average(y2_relative), color="black")
plt.axhline(np.average(y3_relative), color="black")
plt.ylabel("Relative comparison of all PMTs in reference to PMT 1")
plt.title("An example of a UV LED calibration run")
plt.show()  # Creating the specific plot of the UV LED calibration run
```

Figure 28 | A second example of the Python Script that produced figure 26.

2.5. Temperature conditions

2.5.1. Outdoor temperature measurements

The FAST project relies on stable measurements throughout the entire year. As the telescope itself can only operate during clear moonless nights, any observation opportunities have to be utilized, regardless of the season. For that reason, both optical and electrical components have to withstand unfavourable desert conditions of the Pierre Auger Observatory in Argentina. Histogram of outdoor temperature measurements can be seen in figure 29. These measurements have been done by the Dallas DS18B20+ temperature sensor located behind the FAST hut, as seen in figure 17. The operating temperature range of all electrical components as well as the UV LED flasher fall within the range present at the PAO site, which is $\sim$ -10 °C to $\sim$ +37 °C.

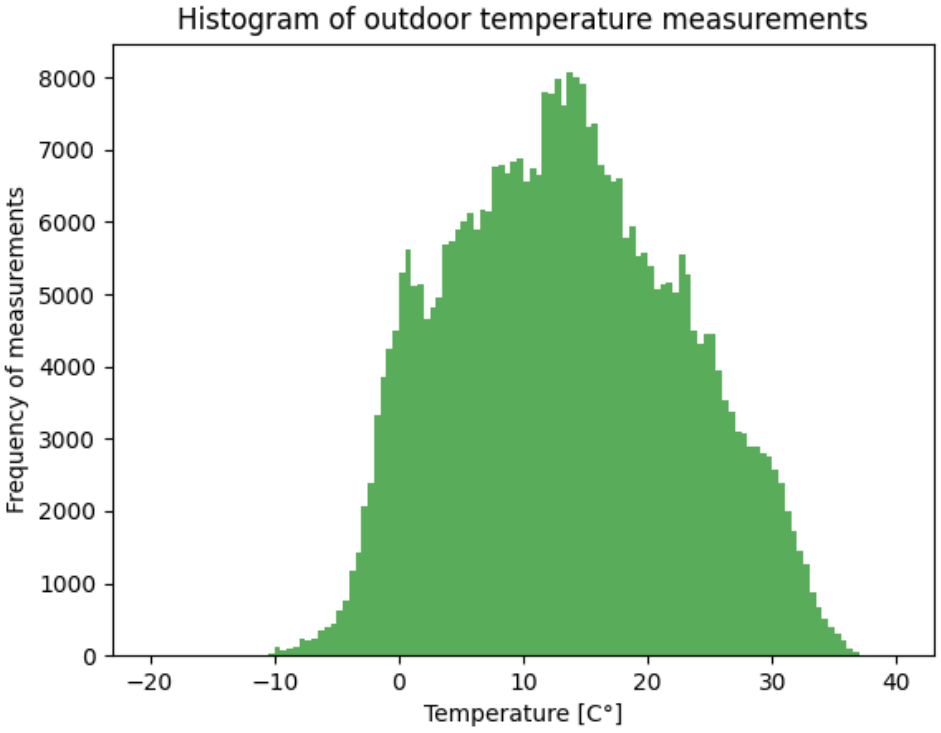

Figure 29 | Outdoor temperature histogram.

The temperature difference could in theory alter the behaviour of the detecting capabilities of the PMTs in addition to the shift of the wavelength of emitted UV light by the UV LED flasher. Such effect however, should only be noticeable in absolute numbers, as temperature fluctuations affect all four PMTs equally. Relative calibration done by comparing signal from all PMTs should produce stable signal values.

2.5.2. Indoor temperature measurements

Indoor temperature readings are of more significance, as they accurately reflect the conditions surrounding the optics and electronics of the FAST telescope. Dallas DS18B20+ temperature sensor located in the rack case provided sufficient measurements of the temperature around the electrical components. The location of this sensor is shown in figure 17. Of vital importance is data acquired from an identical sensor located on the FAST camera box. This temperature detector is the closest to the four 200mm PMTs and data measured by the sensor will be used in relative calibration regarding temperature stability of the PMTs in Section 2.7. Histogram of both rack case temperature and camera temperature measurements can be seen in figures 30 and 31, respectively.

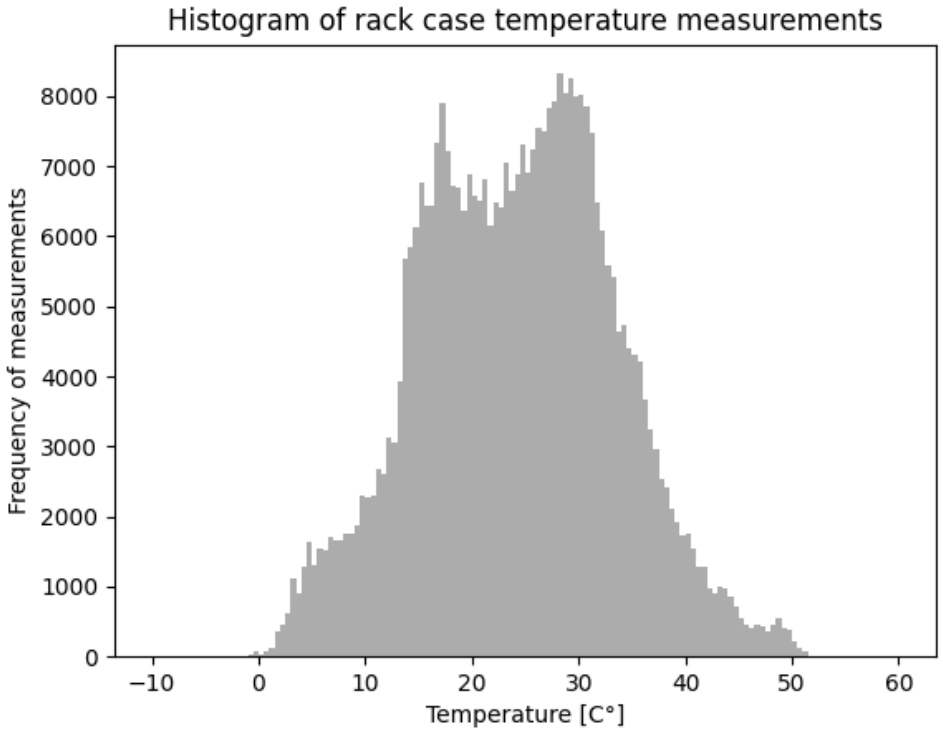

Figure 30 | Rack case temperature histogram.

The rack case histogram seen in figure 30 provides information about the temperature on which the electronics of the FAST telescope operate. The temperature ranges from ~ 0 °C to ~ 50 °C, with a peak at ~ 30 °C. This temperature is well within the operating range of the electrical component present at the FAST telescope.

However, temperature fluctuations could in theory alter the signal gained from all the electrical components as seen in Section 1.6. As the operation of the components is to a degree dependent on temperature, absolute shift in numbers may be present. Nevertheless, such effect should only be noticeable in absolute values, as temperature fluctuations affect the electrical signal from all four PMTs equally. By comparing the individual PMTs on a single FAST telescope, the relative values should in theory stay stabilized.

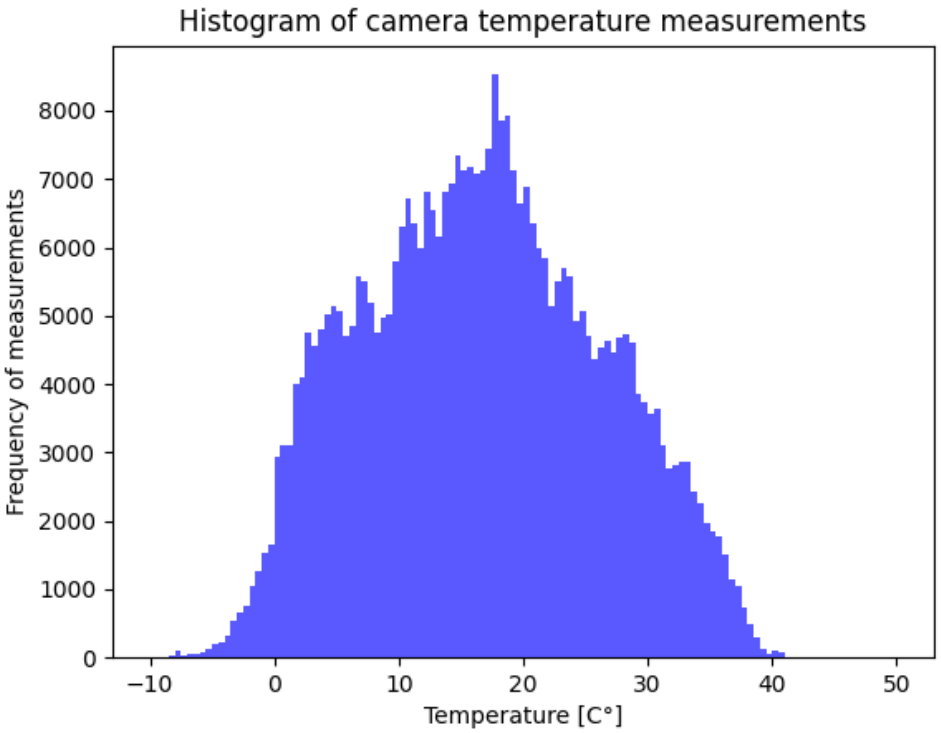

Figure 31 | Camera temperature histogram.

Camera temperature histogram shown in figure 31 provides information about the temperature of the camera box. The temperature ranges from ∼ -8 °C to ∼ +40 °C, with a peak at ∼ 18 °C. This temperature is well within the operating range of the PMTs present on the FAST telescope. For the purpose of subsequent data analysis, these values also represent the temperature of the PMTs.

Temperature fluctuations have drastic effect on the saturation current of the bialkali photocathodes of the PMTs, as described in Section 1.5.2. Decrease in temperature lowers the saturation current, resulting in the loss of linear response of the PMT to incident light. Furthermore, as described in Section 1.6.2 the wavelength of light emitted by the UV LED flasher is also altered. This may result in either decrease or increase in the transmittance rate of the borosilicate glass, from which the input window of the PMT is manufactured. This relation can be seen in figure 18. Nevertheless, any signal fluctuations resulting from such temperature difference should only be noticeable in absolute numbers, as temperature fluctuations affect all four PMTs equally. Relative calibration done by comparing signal from all PMTs should produce stable signal values.

2.5.3. Temperature difference during atmospheric measurements

Temperature stability has to be ensured for proper operation during planned regular UHECR observation. During such measurements, the shutter opens and an influx of cold air can be registered inside the FAST hut. Such rapid temperature discrepancy could in theory alter the properties of both optical and electrical components and in turn alter the signal and hinder the detection of fluorescent UV light produced by an EAS. Data from such measurements is visualized in figures 32 and 33.

Temperature shift could cause signal fluctuations caused by either the decrease or increase in saturation current as described in Section 1.5.2. A time period of one hour is recommended by the manufacturer for the PMT to properly acclimate to surrounding conditions. The vacuum inside the PMTs as seen in figure 11 does not allow for proper heat transfer. More rapid temperature variations could produce inaccurate readings.

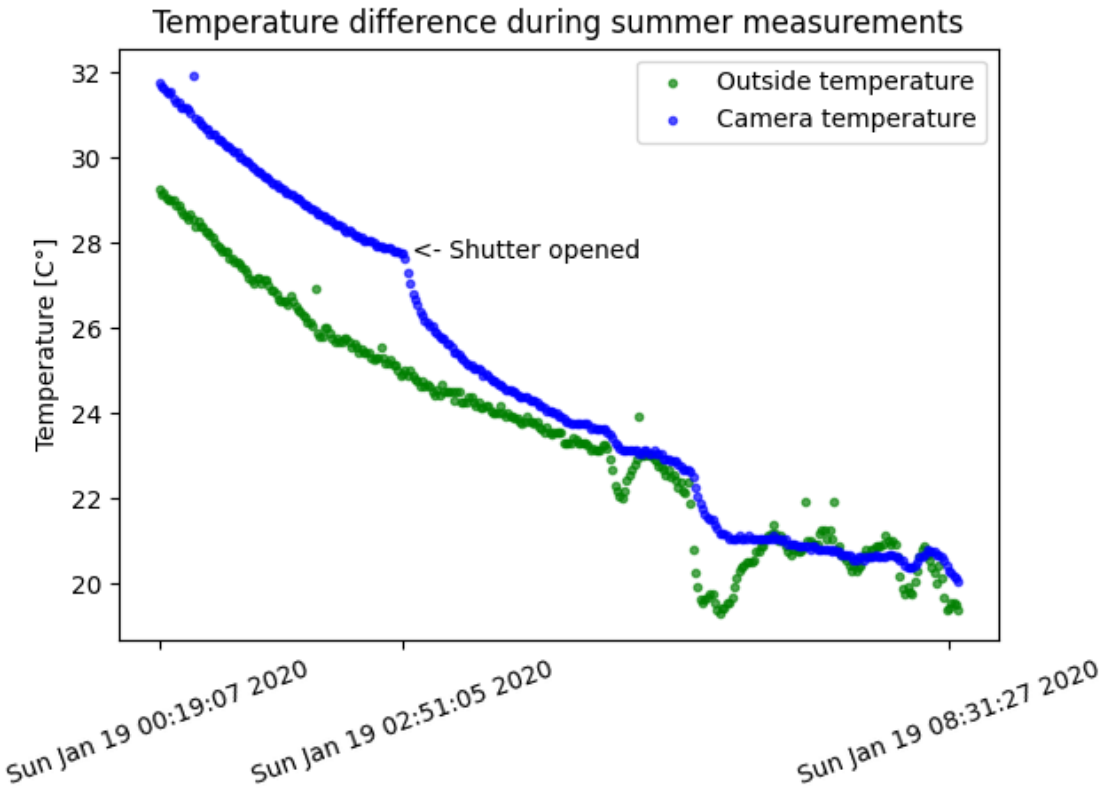

Figure 32 Outdoor and camera temperature difference during atmospheric summer measurements.

During summer measurements, the outdoor and indoor temperature difference amounts to $\sim$ 3 °C. A period of several hours is required for the temperatures to equate. Note that this particular summer measurement occurred in January, as the PAO site in Argentina is located on the southern hemisphere.

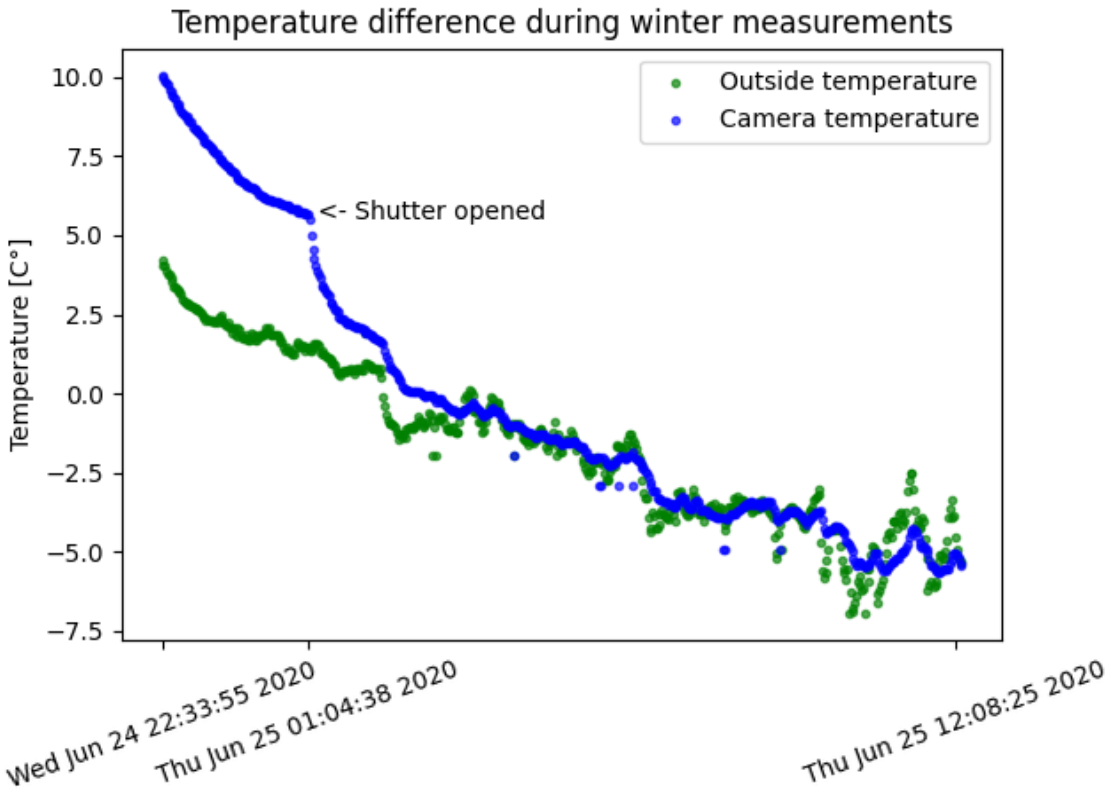

Figure 33 | Outdoor and camera temperature difference during atmospheric winter measurements.

During winter measurements, the outdoor and indoor temperature difference amounts to ~ 4 °C. A period of several hours is required for the temperatures to equate. Disregarding the minor outdoor subsequent temperature fluctuations, after the initial period both temperatures are stabilized. A time interval of several hours provides adequate amount of time for both the optical and electrical components of the FAST telescope to acclimate. This remains the case for either summer or winter measurements.

Moreover, any effect of rapid temperature decrease during shutter opening as seen in figure 33 should only be noticeable in absolute numbers, as the temperature fluctuations affects all four PMTs equally. By comparing the individual PMTs on a single FAST telescope, the relative values should in theory stay stabilized.

2.6. Time stability

Time stability of all four 200mm PMTs is one the primary concerns of data analysis of the UV LED calibration runs. Sufficient optical and mechanical quality and stability have to be ensured for long term accurate observation of UHECR-induced air showers. Significant loss of signal due to material deterioration would severely hinder the detection capabilities of the FAST telescope. The FAST telescope equipped with the UV LED flasher described in Section 1.6.2 is taking calibration measurements since October of 2019. Data until June of 2021 will be examined.

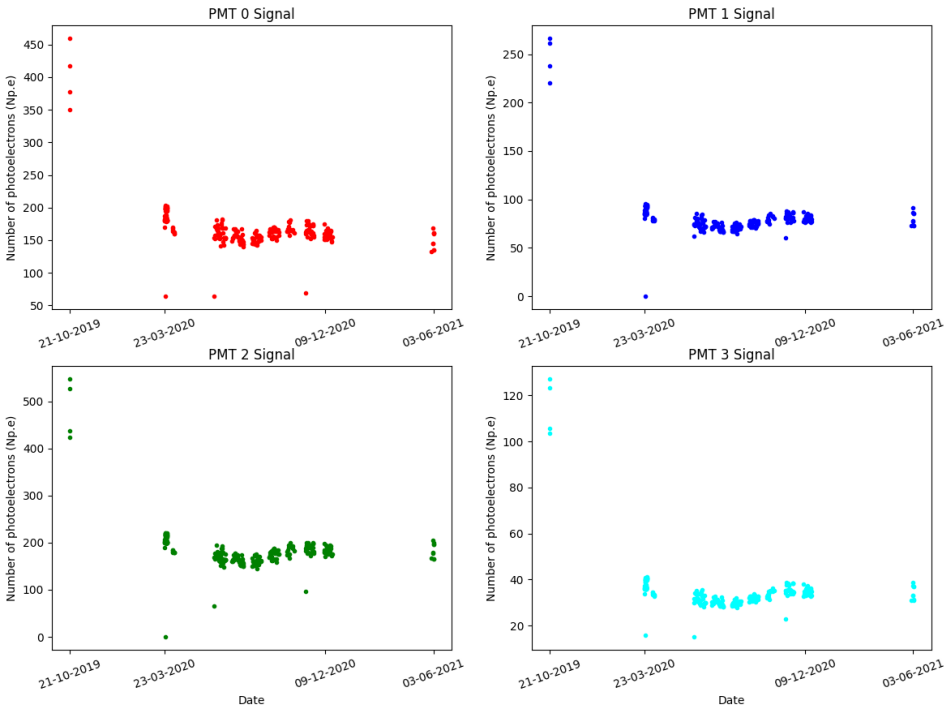

Figure 34 Absolute values of detected number of photoelectrons (Np.e) from the UV LED calibration measurements of the FAST telescope.

Figure 34 shows the absolute signal values measured in the number of photoelectrons (Np.e) from the 21st of October, 2019 until the 3rd of June, 2021. Note that the scale of the y-axis, the number of photoelectrons calculated from the calibration constants, is distinct for each PMT. The signal differs in absolute numbers, nevertheless by comparing the four PMTs with a selected reference point, the relative calibration signal should in theory stay stabilized. Any signal alteration caused for example by environmental conditions, temperature fluctuations or material quality deterioration should affect all four PMTs equally.

A single UV LED calibration cycle provides 5 signal values per PMT. However, for long term analysis all 5 values offer limited significance, as they were measured in an interval of ~ 10 seconds. For that reason only the first value of each calibration run was used.

It is evident that several of the FAST telescope calibration measurement are burdened with an observational error. This is apparent in the signal of PMT 1, as the number of detected photoelectrons should never be zero, provided no defect in the UV LED flasher itself. In addition, unusually low values as seen in signal from PMT 0 for example also indicate a measurement error of a certain kind. This will further be even more visible in figure 35 where relative values of all four PMTs are visualized.

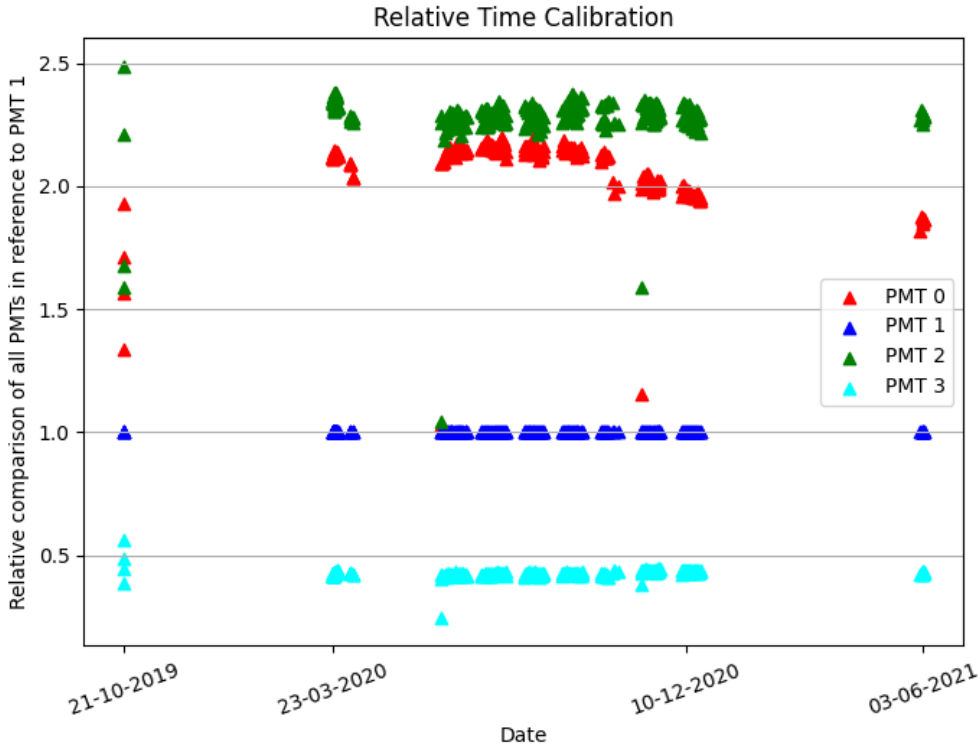

Figure 35 | Relative time calibration visualization with PMT 1 selected as a reference.

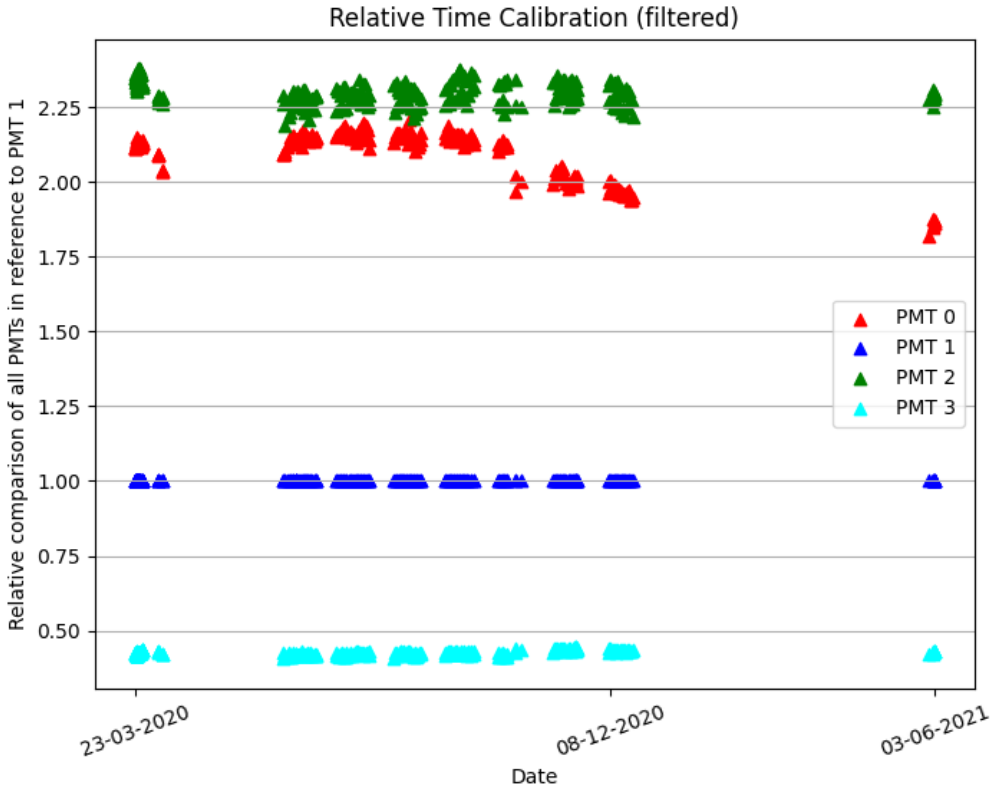

Figure 36 | Relative time calibration visualization with PMT 1 selected as a reference (filtered).

All the values for all PMTs from measurements where PMT 1 detected zero have been removed from the data sheets, as PMT 1 was selected as the reference and division by zero is not feasible for the purpose of relative calibration. Furthermore, figure 35 exposed another set of measurements with noticeable observational errors. All four measurements from the beginning of the run in October, 2019 fall into the category of measurement errors. Exceptionally low values as measured by PMT 0 in figure 34 (top-left) as well. As these values do not provide valuable information towards data analysis and relative calibration they have been removed from the data sheet. Originally, 291 values were present in the calibration run. After the error filter was applied, 284 remained.

PMT 1 shows completely stable signal, as we have compared all the values to this PMT as a reference. Moreover, PMT 3 displays a strong degree of time stability with only minor fluctuations. PMT 0 however, demonstrated a steady downward trend with respect to time. PMT 2 exhibits large fluctuations, but the overall signal remains approximately stable throughout the period of under 2 years of UV LED calibration measurements. Unfortunately, a large data gap caused by the Covid-19 restrictions on site of the observatory is present in the database for the majority of 2020

The subplots of relative calibration with respect to time for the PMTs are shown in figure 37. Note that the absolute values are of no significance for relative calibration, but the range of the graphs is identical for all three compared PMT signals, so fluctuation are more discernible. The black lines on all three subplots represent a mean average value for all three PMTs.

While PMT 3 shows particular time stability throughout the entire UV LED measurement run, PMT 2 displays a large degree of variation of ~ 0.1 with the signal from PMT 1 taken as a reference. Nevertheless, no upward or downward trend is present, in contrast with the case of PMT 0. A significant decrease is noticeable even in relative values towards the end of 2020.

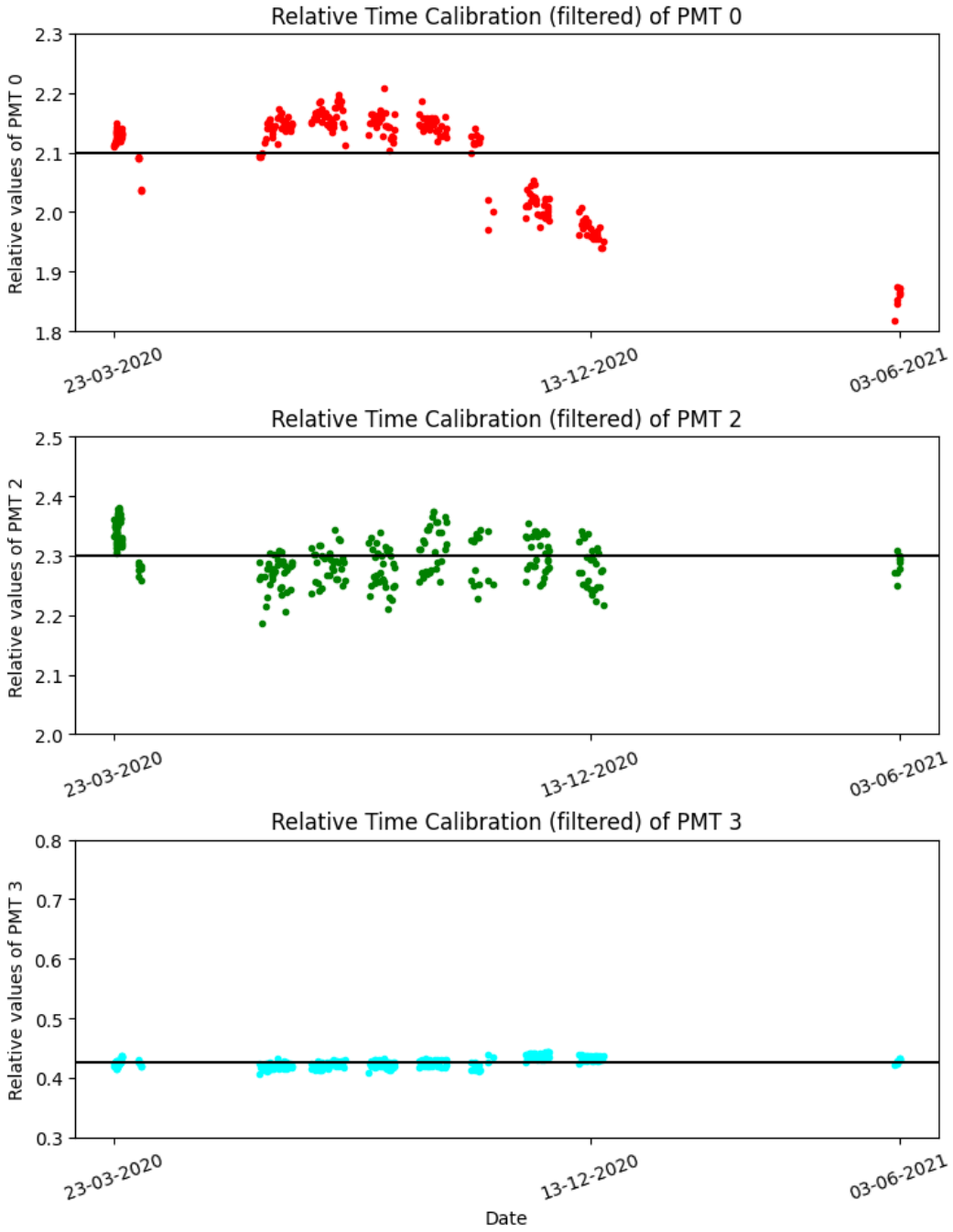

Figure 37 Subplots of relative time calibration from the UV LED calibration measurements for PMT 0 (top), PMT 2 (center) and PMT 3 (bottom) with the signal of PMT 1 taken as a reference (filtered).

2.7. Temperature stability

Temperature stability of all four 200mm PMTs is another primary concern of data analysis of the UV LED calibration runs. As temperature fluctuations definitely alter absolute values of the signal, as explained in section 1.6.2 and 2.5, this effect should only by noticeable in absolute numbers, as temperature variations affect all four PMTs equally. Relative calibration done by comparing signal from all four PMTs should produce stable signal values.

As was the case in section 2.6, only the first measurement of UV LED flash was analyzed, as the $\sim$ 10s time interval between individual UV flashes does not allow for any significant temperature change to affect the PMTs. Furthermore, apparent measurement errors were additionally removed from the calibration data sheet as was the case in relative calibration with respect to time.

To all of the 284 UV LED calibration measurements (after filter application) a single temperature value (°C) was assigned. Data from the Dallas DS18B20+ temperature sensor placed on the camera on the FAST telescope was utilized. The choice for this particular temperature sensor was the maximal proximity to the four PMTs. Figure 38 visualizes the relative calibration signal values from the UV LED measurements with respect to the temperature of the PMTs.

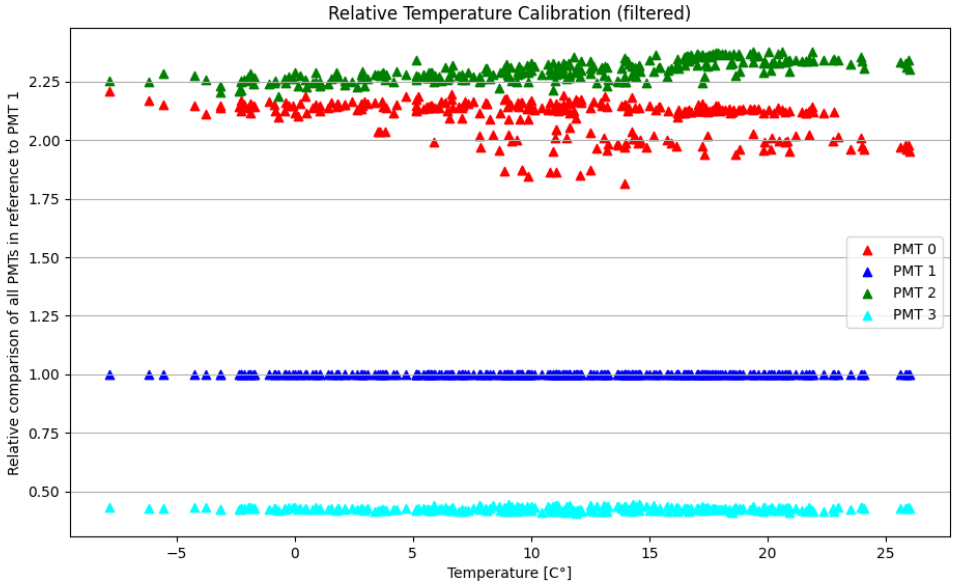

Figure 38 Relative temperature calibration visualization with PMT 1 selected as a reference (filtered).

While PMT 1 displays a completely stable signal, as we have employed this PMT as a reference, PMT 0 and PMT 2 demonstrate a degree of fluctuation. A minor upward trend with increase in temperature can be seen in the relative signal values of PMT 2. PMT 0 exhibits large amount of seemingly random variations with no apparent upward or downward trend.

Detailed subplots of all the PMT signals are shown in figure 39. Note that the absolute values are of no significance for relative calibration, but the range of the graphs is identical for all three compared PMT signals, so fluctuation are more discernible. The black lines on all three subplots represent a mean average value for all three PMTs.

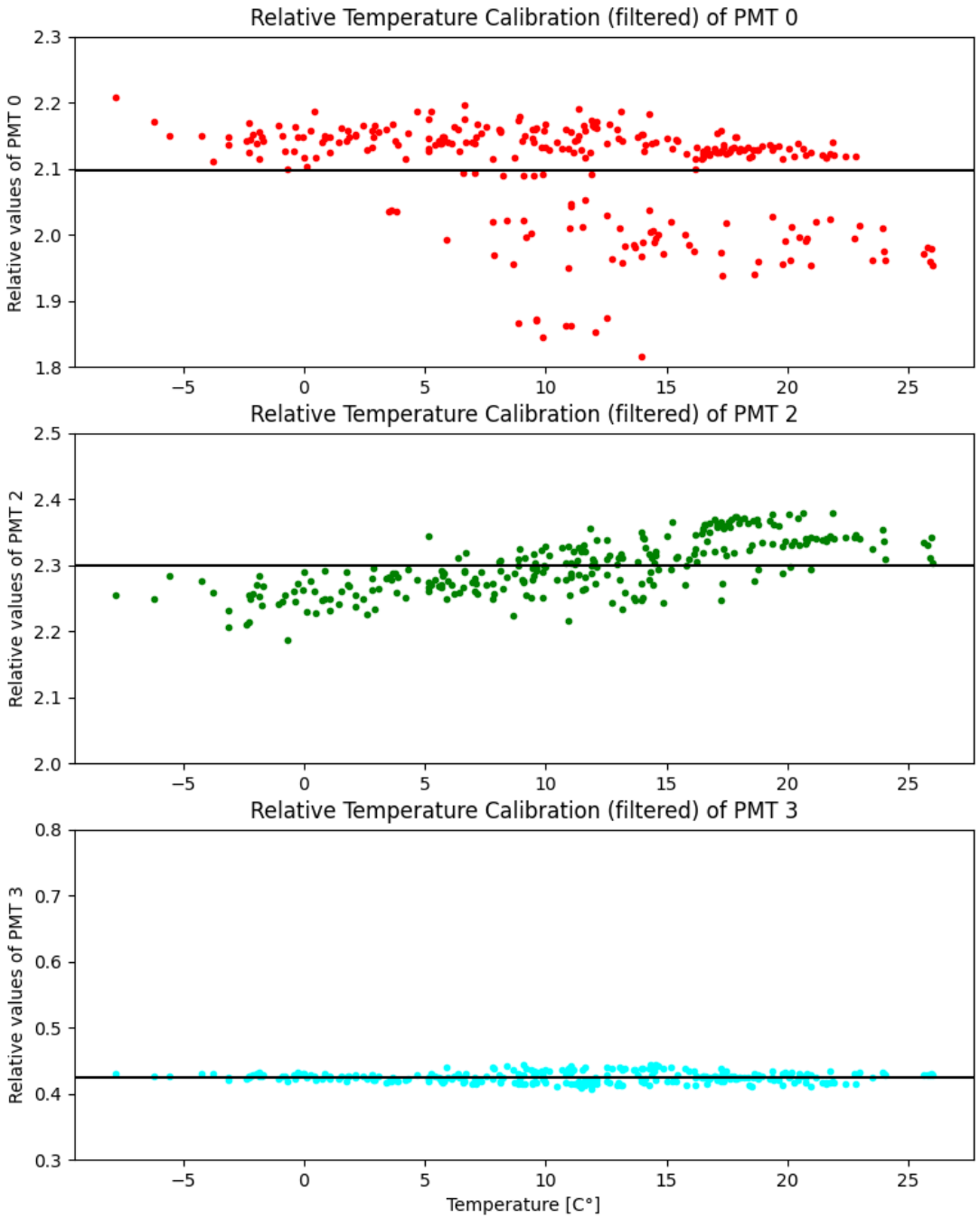

Figure 39 Subplots of relative temperature calibration from the UV LED calibration measurements for PMT 0 (top), PMT 2 (center) and PMT 3 (bottom) with the signal of PMT 1 taken as a reference (filtered).

As the fluctuations of relative signal from PMT 0 with respect to time as seen in figure 37 could in theory cause the fluctuations present in figure 39, visualization of data up until Wednesday, 8th of July 2020 was conducted. During this time period, relative signal values of PMT 0 obtained from UV LED calibration measurements demonstrate a degree of stability with respect to temperature. Figure 40 shows this relation for the limited time interval.

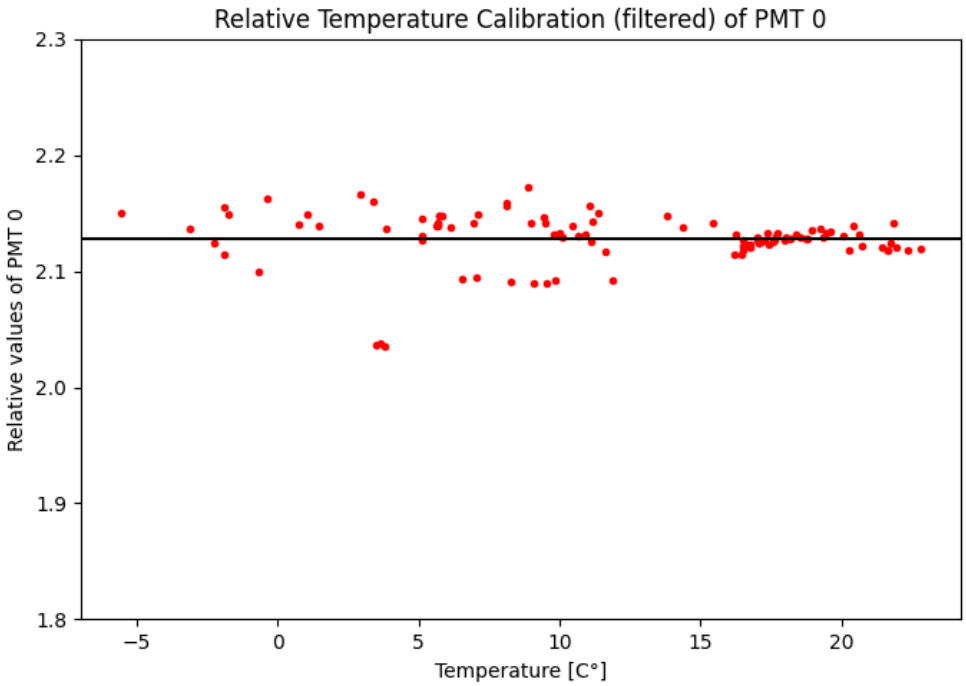

Figure 40 Relative temperature calibration visualization of the signal from PMT 0 with PMT 1 selected as a reference (filtered).

The black line on the image represents a mean average value for relative signal of PMT 0 in reference to PMT 1. While PMT 0 still exhibits relative signal variations, the capacity of the fluctuations is not as significant as the visualization concerning the entire time period, as mention in Section 2.6.

3. Discussion

The FAST telescope contains numerous optical and electrical components that behave distinctly in response to various environmental conditions surrounding them. Temperature fluctuations can for example change the behaviour of the electronics that compose the entire data acquisition system of the FAST telescope. Furthermore, temperature variations alter the optical elements as well. In response to temperature shift, the saturation current changes and loss of linearity may ensue, as shown in figure 15. The UV LED flasher present at all the calibration measurements emits light of slightly different peak wavelength when exposed to temperature change, as can be seen in figure 18. The transmittance of borosilicate glass, the material from which the input window of all four PMTs is manufactured, is also heavily dependent on the wavelength of incident light, as shown in figure 12. In theory, temperature fluctuation can cause the wavelength shift of emitted UV light, which in turn would cause signal change as the transmittance is dependent on wavelength. Moreover, material deterioration may result in the alteration of signal values.

However, all of these effects should only be noticeable in absolute numbers, as all of these variables affect all four PMTs equally. Relative calibration done by comparing signal from all four PMTs should produce stable signal values. None of the aforementioned should in theory be responsible for the behaviour of PMTs that is seen in Section 2.6 and 2.7.

While PMT 3 has shown stability in reference to the UV LED calibration signal of PMT 1, PMT 0 and 2 display a degree of instability in respect to both time and temperature. PMT 0 exhibits a strong decrease in relative signal values from $\sim$ July of 2020 onward. Prior to that time period, no particular downward trend can be observed. Identification of the cause of such behaviour is problematic, as the detector itself is on a different continent and the only available information is the data from the UV LED calibration runs. Rapid material degradation could induce such signal loss. Dust sedimentation or aerosols may be the cause of such behaviour as well. In theory, optical, electrical and material degradation of all PMTs should be identical, but the possibility of a faster, more rapid degradation of particular PMTs cannot be excluded. However, removing the data that produce the downward trend moderately stabilizes the PMT 0 signal with respect to temperature. Whether such effects have caused instability with respect to temperature, or whether this is entirely a separate issue, is unknown. Additional in-situ testing should be provided using e.g. calibrated light source of Yttrium-Aluminum Perovskite (YAP) pulser. However, the demand of on site observation cannot be accomplished due to the current Covid-19 restrictions. Alternatively, measurements could be done in a lab using proper instrumentation (ordered in July of 2020, not yet delivered).

Signal from PMT 2 displays an ascending trend correlated with the increase in temperature, as shown in figure 39. In theory all four PMTs should respond to temperature variations equally, however the option that individual PMTs can be more sensitive to temperature change cannot be excluded. Material degradation can as well be involved in inducing such behaviour. Whether the observed upward trend with respect to temperature is also responsible for the fluctuations present in figure 37 for PMT 2 is unknown. No reasonable assumption as to the culprit of such signal alterations can be made by only analysing the UV LED calibration measurements.

It is important to note that both PMTs that exhibit a degree of instability, PMT 0 and PMT 2, are situated on the same vertical plane. Whether this is a coincidence or this plays a role in signal values is up for debate. Dust sedimentation could produce such behaviour, as the dust should affect PMT 0 and PMT 2 more, because they are set on a higher vertical plane compared to the two remaining PMTs. The FAST telescope should be protected from dust and aerosols by the UV aperture filter and the shroud. Without examining the components physically, no reasonable assumption as to the cause of such instability can be made.

Conclusion and outlook

The Fluorescence detector Array of Single-pixel Telescopes is a concept for next generation observatory of ultra high-energy cosmic radiation. Because of the exceptionally low flux of such radiation, a large net has to be deployed to obtain a statistical sample of reasonable size for proper analysis. The FAST telescope offers an aperture collecting area of ~ 1 m^2 and a FOV of $30° \times 30°$. The low economic cost and simple transportation and installation make these detectors ideal for detecting UHECRs. The detection is done by observing faint fluorescent UV light produced in the atmosphere by deexcitation of nitrogen atoms during the cascade of secondary particles induced by the UHECR. The aperture of the FAST telescope is covered with a UV filter and the entire structure is protected by a shroud to eliminate any parasitic background light. The segmented "petal" shaped mirror reflects the UV photons onto a camera box containing four 200mm Photomultiplier Tubes.

The FAST telescope present at the Pierre Auger Observatory in Argentina is equipped with a UV LED flasher. This UV LED serves to provide measurements useful in calibration of the telescope itself. Furthermore, the data acquisition system is provided with numerous sensor detecting outdoor, indoor or camera temperature, humidity or closure of the shutter. All the data is then stored on a MariaDB database in Joint Laboratory of Optics of the Palacky University, Czech republic.

Several environmental conditions could impact the signal from both the optical and electrical instruments of the FAST telescope. However, such signal fluctuations should only by noticeable in absolute numbers, as the conditions affect all four PMTs equally. Relative calibration done by comparing signal from all four PMTs should produce stable signal values. PMT 3 displayed a large amount of stability with the signal from PMT 1 chosen as a reference. PMT 0 and PMT 2 both exhibit fluctuations with respect to time and temperature. A downward trend is observed with PMT 0 with respect to time and an upward trend is observed with the signal from PMT 2 with respect to temperature. By filtering data from July, 2020 onward the data from PMT 0 demonstrate moderate stability with respect to temperature. The cause of this behaviour is unknown. Rapid material degradation or dust sedimentation may induce such fluctuations. Lacking physical evidence no reasonable assumptions can be made towards the cause. Summary on the complete stability of the four PMTs is shown in a histogram in figure 41.

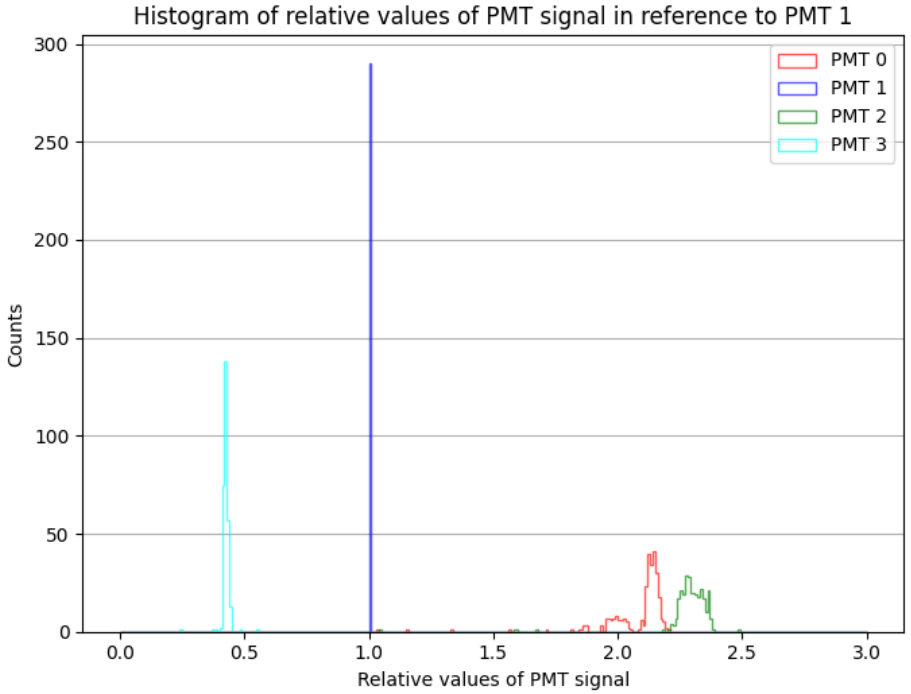

Figure 41 | Histogram of relative signal values of all four PMTs in reference to PMT 1.

To better understand the behaviour of the PMTs present on the FAST telescope more data and a larger study is required. Remote control of the UV LED flasher is planned. Ability to remotely regulate the power of the flasher would provide sufficient measurements in order to obtain information about linearity of the flasher and signal from all four PMTs.

Measurement in a constant climate chamber would supply the FAST collaboration with information about the stability of PMT signal in respect to time, as the environmental conditions such as temperature, humidity and pressure should stay constant.

The light from the UV LED flasher is not constant as well. Measurements regarding homogeneity of emitted light is crucial to better understand the UV LED calibration data. Such knowledge of the flasher is vital to calibrate the individual PMTs.

The FAST project successfully demonstrated its viability in detecting UHECRs through faint fluorescent UV light produced by an EAS. To ensure accurate and precise measurements for any statistical and physical relevance, calibration of the four PMTs present on the FAST telescope has to be guaranteed. Relative calibration aims to compare the signal of the PMTs with one of them chosen as a reference. For proper operation, absolute calibration has to be maintained. Conditions such as temperature, humidity, pressure, cloud coverage or material deterioration alter the detection capabilities of aforementioned telescope. These conditions have to be monitored and corrections for their effects have to be performed. To maximize the amount of observation time, the telescope operates throughout the entire year and is thus subjected to various conditions. Measurements containing information about the behaviour of PMTs signal in response to such conditions is vital for absolute calibration of the FAST telescopes.

References

[1] Bietenholz, Wolfgang. *"The most powerful particles in the Universe: a cosmic smash."*, 2013. https://arxiv.org/abs/1305.1346

[2] R.A. Mewaldt, *Galactic cosmic ray composition and energy spectra, Advances in Space Research, Volume 14*, Issue 10, 1994, Pages 737-747, ISSN 0273-1177. https://doi.org/10.1016/0273-1177(94)90536-3

[3] M. S. Pshirkov, P. G. Tinyakov, F. R. Urban, *Mapping ultrahigh energy cosmic rays deflections through the turbulent galactic magnetic field with the latest rotation measure data, Monthly Notices of the Royal Astronomical Society*, Volume 436, Issue 3, 11 December 2013, Pages 2326–2333. https://doi.org/10.1093/mnras/stt1731

[4] Telescope Array (TA), Utah - USA, (cit. 26.7.2021). http://www.telescopearray.org/

[5] Pierre Auger Observatory (PAO), Argentina, (cit. 26.7.2021). https://www.auger.org/

[6] Mandat Dusan, M. Palatka, M. Pech, P. Schovanek, P. Travnicek, L. Nozka, M. Hrabovsky et al. *"The prototype opto-mechanical system for the Fluorescence detector Array of Single-pixel Telescopes."Journal of Instrumentation 12*, no. 07 (2017): T07001. https://iopscience.iop.org/article/10.1088/1748-0221/12/07/T07001

[7] Malacari M., et al. *"The first full-scale prototypes of the fluorescence detector array of single-pixel telescopes."Astroparticle Physics*, 119 (2020): 102430. https://doi.org/10.1016/j.astropartphys.2020.102430

[8] T. Fujii et al, *Detection of ultra-high energy cosmic ray showers with a single-pixel fluorescence telescope, Astroparticle Physics*, Volume 74, 2016, Pages 64-72, ISSN 0927-6505. https://doi.org/10.1016/j.astropartphys.2015.10.006

[9] Cattaneo, Paolo Walter. *"Optical analysis of spherical mirrors of telescopes: The lens-less Schmidt case."Nuclear Instruments and Methods in Physics Research Section A: Accelerators, Spectrometers, Detectors and Associated Equipment*, 608, no. 3 (2009): 384-389. https://ui.adsabs.harvard.edu/link_gateway/2009NIMPA.608..384C/doi:10.1016/j.nima.2009.07.032

[10] Pech Miroslav, Justin Albury, Jose A. Bellido, John Farmer, Toshihiro Fujii, Petr Hamal, Pavel Horvath et al. *"Simulation of the optical performance of the Fluorescence detector Array of Single-pixel Telescopes."* In EPJ Web of Conferences, vol. 210, p. 05014. EDP Sciences, 2019. https://doi.org/10.1051/epjconf/201921005014

[11] Hamamatsu Photonics K.K, *Photomultiplier Tubes, Basics and Application* (*edition 3a*). https://www.hamamatsu.com/resources/pdf/etd/PMT_handbook_v3aE.pdf

[12] Roithner LaserTechnik, *Technical Data, RLT365-10E*. Available at http://www.roithner-laser.com/datasheets/led_div/rlt365-10e.pdf

[13] DBeaver, free multi-platform tool for database viewing. https://dbeaver.io/

[14] Python Software Foundation. Python Language Reference, version 3.9. Available at http://www.python.org

[15] Jetbrains, Integrated development environment PyCharm, version 2021.1.3. Available at https://www.jetbrains.com/pycharm/

[16] Harris, C.R., Millman, K.J., van der Walt, S.J. et al. *Array programming with NumPy. Nature*, 585, 357–362 (2020). https://doi.org/10.1038/s41586-020-2649-2

[17] J. D. Hunter, *"Matplotlib: A 2D Graphics Environment"*, *Computing in Science & Engineering*, vol. 9, no. 3, pp. 90-95, 2007. https://doi.org/10.1109/MCSE.2007.55

[18] Michael Bayer. SQLAlchemy. In Amy Brown and Greg Wilson, editors, *"The Architecture of Open Source Applications Volume II: Structure, Scale, and a Few More Fearless Hacks"*, 2012. http://aosabook.org

List of abbreviations

FAST	Fluorescence detector Array of Single-pixel Telescopes
UHECR	Ultra high-energy cosmic radiation
EAS	Extensive air shower
TA	Telescope Array
PAO	Pierre Auger Observatory
FOV	Field of vision
PMT	Photomultiplier tube
eV	Electronvolt
UV	Ultraviolet
BRM	Black Rock Mesa
LP	Low-pass
FADC	Fast analog-to-digital converter
DAQ	Data Acquisition
RPi4	Raspberry Pi 4
Np.e	Number of photoelectrons
YAP	Yttrium-Aluminum Perovskite